Hadronic loop effects on the radiative decays of the first radial excitations of η and η'

Yin Cheng[*] and Qiang Zhao[†]

Institute of High Energy Physics, Chinese Academy of Sciences, Beijing 100049, People's Republic of China and University of Chinese Academy of Sciences, Beijing 100049, People's Republic of China

(Received 25 June 2021; revised 24 February 2022; accepted 5 April 2022; published 29 April 2022)

Based on the one-state assumption of $\eta(1405)$ and $\eta(1475)$, $\eta(1295)$ and $\eta(1405/1475)$ thus being organized as the first radial excitations of η and η', respectively, we investigate the productions and radiative decays of these two states in $J/\psi \to \gamma\eta_X \to \gamma\gamma V$, where η_X stands for $\eta(1295)$ and $\eta(1405/1475)$ and V stands for vector mesons ρ^0, ω, ϕ. As we have learned from previous studies that the hadronic decays of these two states receive important contributions from the intermediate $\bar{K}K^* + \text{c.c.}$ meson loops due to the triangle singularity mechanism, we show that some measurable effects can also arise from the $\bar{K}K^* + \text{c.c.}$ meson loops in their radiative decays. Our calculation shows that the impact of the $\bar{K}K^* + \text{c.c.}$ meson loops on the $\eta(1405/1475)$ radiative decays is relatively smaller than on $\eta(1295)$ since the latter has a much larger coupling to $\bar{K}K^* + \text{c.c.}$ However, the production of $\eta(1295)$ in the J/ψ radiative decays will be strongly suppressed due to its being the radial excitation state of the η meson. As a consequence of the $\bar{K}K^* + \text{c.c.}$ meson loop contributions, we find that the mixing angle extracted in the radiative decays of $\eta(1295)$ and $\eta(1405/1475)$ will be different from each other, and both are different from the one determined in other processes.

DOI: 10.1103/PhysRevD.105.076023

I. INTRODUCTION

The study of flavor singlet and octet mixing in the lightest pseudoscalar nonet, i.e., between η and η', has attracted a lot of attention in the history. As it has been well established that the $U(1)_A$ anomaly is the driving mechanism for many interesting phenomena for these two states, it also raises interesting questions on its role for higher radial excitation states in the isoscalar pseudoscalar spectrum, in particular, the first radial excitation states. The present experimental data for the $J^{P(C)} = 0^{-(+)}$ spectrum are still far from satisfactory. For the first radial excitation, there are enough states to fill a nonet between 1.25 $\sim$ 1.50 GeV, which includes $\pi(1300)$, $K(1460)$, $\eta(1295)$, and $\eta(1405)/\eta(1475)$ [1]. But for higher excitations, the experimental evidences are far from well established.

Even for the first radial excitations, one can see that the question of whether there are two states, $\eta(1405)$ and $\eta(1475)$, present in the same mass region would have strong impact on our understanding of low-energy QCD phenomena. Historically, the first evidence for $\eta(1405)/\eta(1475)$ was from $p\bar{p}$ annihilations at rest into $(K\bar{K}\pi)\pi^+\pi^-$ [2], where a pseudoscalar of $J^{PC} = 0^{-+}$ was seen in the invariant mass spectrum of $K\bar{K}\pi$. As an SU(3) partner of the lighter pseudoscalar $\eta(1295)$, it shows that its production strength in $p\bar{p}$ annihilations is much larger than $\eta(1295)$. This was regarded as evidence for its unusual flavor contents in the literature (see, e.g., Ref. [3] for a review). Later, MARK III [4] and DM-2 [5] reported possible two-state structures around 1.44 GeV mass region with increased statistics. The Obelix Collaboration at LEAR [6] seemed to confirm the MARK III result and introduced two pseudoscalars, i.e., $\eta(1405)$ and $\eta(1475)$, in the description of the invariant mass spectrum of $\eta\pi\pi$ [7]. The splitting of one state $\eta(1440)$ into two states, $\eta(1405)$ and $\eta(1475)$, suggested an outnumbering of the SU(3) nonet and could be an indication of exotic hadrons beyond the conventional quark model. In line of this possibility, there was theoretical expectation from the flux tube model that the ground-state pseudoscalar glueball should have a mass around 1.4 GeV [8]. It made one of these two close states, $\eta(1405)$ and $\eta(1475)$, a possible candidate for the pseudoscalar glueball and initiated a lot of efforts on understanding their structures [9–14]. In such a scenario,

[*]chengyin@ihep.ac.cn
[†]zhaoq@ihep.ac.cn

Published by the American Physical Society under the terms of the Creative Commons Attribution 4.0 International license. Further distribution of this work must maintain attribution to the author(s) and the published article's title, journal citation, and DOI. Funded by SCOAP[3].

its mixing with the ground states η and η' become an interesting topic in phenomenology, although the gluon contents inside η and η' cannot be dramatically large [15–17].

While the signal for the heavier one turned out to be more clear in the $K\bar{K}\pi$ channel, and the lighter one seemed to favor the $\eta\pi\pi$ channel, $\eta(1405)$ has been assigned as the pseudoscalar glueball candidate, while $\eta(1475)$ was assigned as the SU(3) partner of $\eta(1295)$ (see, e.g., the minireviews on non-$q\bar{q}$ mesons in early editions of Particle Data Group (PDG) since 1990). However, the glueball assignment with a low mass around 1.4 GeV is not supported by the lattice QCD (LQCD) simulations which came to the playground later. Both quenched [18–21] and unquenched calculations [22,23] suggest that the ground-state pseudoscalar glueball should have a mass around 2.4–2.6 GeV. In experiment, more and more high-precision data from J/ψ and $\psi(3686)$ decays at BESIII were published during the past decade. There is no indication that two pseudoscalar states $\eta(1405)$ and $\eta(1475)$ are needed in the description of any exclusive channel such as $\eta\pi\pi$ [24–26], $K\bar{K}\pi$ [27], and the isospin-violating 3π channel [28]. Interestingly, it seems to be true that the pseudoscalars observed in different channels have slightly shifted masses. For instance, the mass extracted in the $K\bar{K}\pi$ channel is 1452.7 ± 3.8 MeV [27], while the masses in $\eta\pi\pi$ and 3π are about 1405 MeV [24–26,28].

A breakthrough of the puzzling situation was the proposal by Ref. [29] in the interpretation of the abnormally large isospin-breaking effects observed by BESIII in $J/\psi \to \gamma\eta(1405/1475) \to \gamma + 3\pi$ [28]. The interference from the intermediate $K^*\bar{K} + \text{c.c.}$ rescattering via a triangle loop can contribute to the isospin breaking at leading order due to the satisfaction of the triangle singularity (TS) condition [30–33]. The TS mechanism can naturally explain the mass shift and decay patterns with only one state around 1.4 GeV [29,34,35]. Further detailed studies including the width effects were also investigated in the literature [36,37]. In Ref. [36], it was claimed that the TS contribution would be suppressed by the width effects of the intermediate K^*. Therefore, the TS mechanism may not be sufficient for accounting for the large isospin-breaking effects observed by BESIII [28]. A comprehensive analysis in Ref. [37] later showed that one important transition process via the TS mechanism was overlooked by the previous analyses. The TS mechanism can also enhance the direct production of $a_0(980)$ in the isospin-conserving channel and then enhance the isospin-violating channel via the $a_0(980)$-$f_0(980)$ mixing. The analysis of Ref. [37] thus firms up the role played by the TS mechanism in the understanding of the $\eta(1405)$ and $\eta(1475)$ puzzle.

It should be mentioned that in phenomenological studies of the pseudoscalar glueball mixing with the $q\bar{q}$ states, i.e., η-η'-G or η-η'-G-η_c mixings, the physical mass of the pseudoscalar glueball was assigned by $\eta(1405)$. By doing so, the gluon contents introduced into η and η' seem to agree with the experimental observables. However, as shown by a detailed analysis of Ref. [17] following the axial vector anomaly dynamics [15,16], the gluon contents inside η and η' are not sensitive to the physical mass of the pseudoscalar glueball. Furthermore, with the LQCD pure gauge glueball mass as an input, the physical mass cannot get to be lighter than 1.8 GeV [17]. A similar conclusion was found by Refs. [38,39] in the framework of the axial vector anomaly.

Motivated by this progress on disentangling the $\eta(1405)$ and $\eta(1475)$ puzzle, we will investigate the scenario of treating $\eta(1295)$ and $\eta(1405)$ [hereafter, we use $\eta(1405)$ to denote all signals related to either $\eta(1405)$ or $\eta(1475)$ in the previous two-state scenario] as the first radial excitation states of η and η'. The radiative decay of $\eta(1405) \to \gamma\rho$ and $\eta(1405) \to \gamma\phi$ have been measured by BES-II [40] and BESIII collaborations [41], respectively, in the J/ψ radiative decays. We will systematically study $J/\psi \to \gamma\eta_X \to \gamma\gamma V$ with $\eta_X = \eta(1295)$; $\eta(1405)$; and $V = \phi, \rho^0, \omega$ and examine the role played by the intermediate $K^*\bar{K}$ meson loops. This should provide further experimental evidence for the one-state solution for $\eta(1405)$ and $\eta(1475)$ and allow a natural categorization of $\eta(1295)$ and $\eta(1405)$ as the first radial excitation states of η and η'.

To proceed, we first introduce the mixing between the SU(3) flavor singlet and octet and then present the formalism for $J/\psi \to \gamma\eta_X \to \gamma\gamma V$ in the framework of the vector meson dominance (VMD) model in Sec. II. We stress that this will allow a self-consistent calculation of both tree-level transitions and loop corrections of the radiative decays of $\eta_X \to \gamma V$. In Sec. III, we will present our numerical results for measurable branching fractions and discuss their phenomenological consequences. A brief summary will be given in Sec. IV. In the Appendix, the loop functions for each loop transition amplitude are provided.

II. FORMALISM

A. Flavor singlet and octet mixing and parametrization for the production mechanism

As the first radial excitation of η and η', $\eta(1295)$ and $\eta(1405)$ can be expressed on the quark-flavor basis similar to η-η',

$$\begin{aligned} \eta(1295) &= \cos\alpha_P n\bar{n} - \sin\alpha_P s\bar{s}, \\ \eta(1405) &= \sin\alpha_P n\bar{n} + \cos\alpha_P s\bar{s}, \end{aligned} \tag{1}$$

where $n\bar{n} \equiv (u\bar{u} + d\bar{d})/\sqrt{2}$ and $\alpha_P \equiv \arctan\sqrt{2} + \theta_p$ with θ_p the flavor singlet and octet mixing angle. Whether the mixing angle is the same as that for the η-η' mixing is still an open question. In Ref. [42], Isgur proposed that, although the η-η' mixing angle deviated from the ideal mixing significantly, the higher states should restore the

ideal mixing angle, given that the mass difference between the flavor $n\bar{n}$ and $s\bar{s}$ could be neglected. In this study, we can either leave the mixing angle to be determined by experimental data or test the results by adopting the same mixing angle as that for η-η'.

Taking the advantage of the antisymmetric tensor structure of the VVP coupling, we can parametrize the coupling strength for $J/\psi \to \gamma(q\bar{q})_{0^{-+}}$, where $(q\bar{q})_{0^{-+}}$ stands for a light isoscalar quark-antiquark pair produced in the J/ψ radiative decays, as

$$g_0 \equiv \langle (q\bar{q})_{0^{-+}} | \hat{H}_\gamma | J/\psi \rangle, \tag{2}$$

where $\hat{H}_\gamma$ represents the corresponding potential for the production of $(q\bar{q})_{0^{-+}}$. Based on the SU(3) flavor symmetry, the coupling strengths $\tilde{g}_{\eta_X}$ can be written as

$$\begin{aligned} \tilde{g}_{\eta(1295)} &= g_0(\sqrt{2}\cos\alpha_P - R\sin\alpha_P), \\ \tilde{g}_{\eta(1405)} &= g_0(\sqrt{2}\sin\alpha_P + R\cos\alpha_P), \end{aligned} \tag{3}$$

for $\eta(1295)$ and $\eta(1405)$, respectively. In the above equation, R is an SU(3) flavor symmetry-breaking parameter. It distinguishes the production of an $s\bar{s}$ from $u\bar{u}$ and $d\bar{d}$ and generally takes $R \simeq m_{u/d}/m_s$.

It is clear here that the production of $\eta(1295)$ would be highly suppressed in comparison with the production of $\eta(1405)$ due to the destructive interference between the $n\bar{n}$ and $s\bar{s}$ component for $\eta(1295)$ and constructive interference for $\eta(1405)$ in the radial excitation scenario if the same mixing angle as that for the η-η' mixing is adopted. This is consistent with the current experimental observation that signals for $\eta(1405)$ are much stronger than for $\eta(1295)$ [1].

Under the assumption, the ratio of $\Gamma(J/\psi \to \gamma\eta(1405))$ to $\Gamma(J/\psi \to \gamma\eta(1295))$ can be expressed as

$$\frac{\Gamma(J/\psi \to \gamma\eta(1405))}{\Gamma(J/\psi \to \gamma\eta(1295))} = \left(\frac{|\mathbf{p}_{\eta(1405)}|}{|\mathbf{p}_{\eta(1295)}|}\right)^3 \times \left(\frac{\sqrt{2}\sin\alpha_P + R\cos\alpha_P}{\sqrt{2}\cos\alpha_P - R\sin\alpha_P}\right)^2, \tag{4}$$

where the partial momentum has been included in these two P-wave processes. In principle, experimental data for exclusive decay branching ratios will determine g_0, and the relation in Eq. (4) will provide a test of the radial excitation picture as α_P and R will share the same values as for η and η' [43,44]. However, to extract the J/ψ exclusive decay branching ratios, one has to subtract the decay information of the intermediate pseudoscalar mesons in $J/\psi \to \gamma\eta_X \to \gamma\gamma V$. As shown in Table I, so far, the most precise data from BESIII are still combined branching ratios. It means that a better understanding of the η_X exclusive decay into γV is required.

The effective couplings for $\eta_X \to \gamma V$ are defined as

$$\mathcal{L}_{\eta_X\gamma V} = g_{\eta_X\gamma V}\epsilon_{\alpha\beta\delta\lambda}\partial^\alpha V^\delta \partial^\beta A^\lambda P, \tag{5}$$

where $g_{\eta_X\gamma V}$ contains the contributions from all possible mechanisms in $\eta_X \to \gamma V$ and the electromagnetic (EM) field A^λ contains both isoscalar and isovector components. At the hadronic level, the effective coupling can be decomposed into the tree diagram contributions via the VMD model and meson loop transitions as higher-order corrections. The transition mechanism is illustrated by Fig. 1. Notice that the coupling vertices are well defined in the SU(3) flavor symmetry limit. The detailed calculations of the tree and loop amplitudes will be given in the next subsection. With the calculated $g_{\eta_X\gamma V}$, one can express the partial decay width for $J/\psi \to \gamma\eta_X \to \gamma\gamma V$ as

$$\begin{aligned} \Gamma_{J/\psi\to\gamma\eta_X\to\gamma\gamma V} \propto \int \frac{d^3\mathbf{p_1}d^3\mathbf{p_2}d^3\mathbf{p_3}}{(2\pi)^9 2E_1 2E_2 2E_3}(2\pi)^4\delta^4(P_{J/\psi} - p_1 - p_2 - p_3) \\ \times \{\tilde{g}_{\eta_X} g_{\eta_X\gamma V}[G_{\eta_X}(s = (p_2+p_3)^2) + G_{\eta_X}(s = (p_1+p_3)^2)]\}^2 2s \times 2m_{J/\psi}^2 |\mathbf{p_1}|^2 |\mathbf{p_2}|^2, \end{aligned} \tag{6}$$

TABLE I. Branching ratios of the combined decays of $J/\psi \to \gamma\eta(1405/1475)$ and $\eta(1405/1475)$ decays into final states. For $J/\psi \to \gamma\eta(1405) \to \gamma\gamma\phi$, two solutions are provided by the BESIII analysis [41].

Channel	Branching ratio
$\mathrm{BR}(J/\psi \to \gamma\eta(1405/1475) \to \gamma K\bar{K}\pi)$	$(2.8 \pm 0.6) \times 10^{-3}$ [45]
$\mathrm{BR}(J/\psi \to \gamma\eta(1405/1475) \to \gamma\gamma\rho)$	$(7.8 \pm 2.0) \times 10^{-5}$ [45]
$\mathrm{BR}(J/\psi \to \gamma\eta(1405/1475) \to \gamma\gamma\phi)(I)$	$(7.03 \pm 0.92 \pm 0.91) \times 10^{-6}$ [41]
$\mathrm{BR}(J/\psi \to \gamma\eta(1405/1475) \to \gamma\gamma\phi)(II)$	$(10.36 \pm 1.51 \pm 1.54) \times 10^{-6}$ [41]

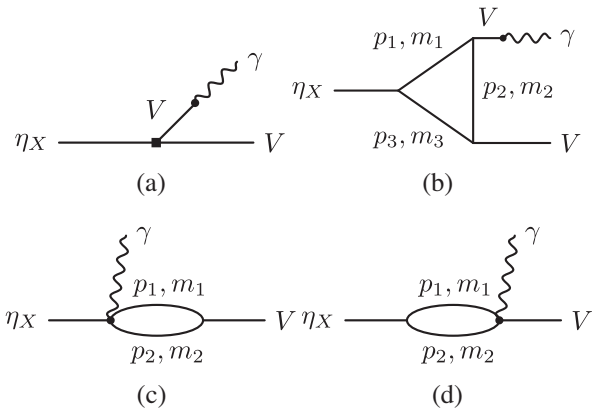

FIG. 1. Schematic diagrams for the process $\eta_X \to \gamma V$ at the tree and loop levels in the VMD model. Part (a) stands for the tree-level transitions; part (b) stands for the hadronic triangle loop transitions; and parts (c) and (d) denote the contact diagrams with a photon induced by the minimum substitution at the two strong interaction vertices, respectively.

where $P_{J/\psi}$ is the 4-vector momentum of the initial J/ψ; $G_{\eta_X}(s)$ denotes the propagator of $\eta(1405)$ or $\eta(1295)$, respectively, i.e.,

$$G_{\eta(1405)}(s) = \frac{i}{s - m^2_{\eta(1405)} + i m_{\eta(1405)}\Gamma_{\eta(1405)}},$$
$$G_{\eta(1295)}(s) = \frac{i}{s - m^2_{\eta(1295)} + i m_{\eta(1295)}\Gamma_{\eta(1295)}}. \quad (7)$$

Note that the parametrization of Eq. (6) has neglected the energy or momentum dependence with the couplings $\tilde{g}_{\eta_X}$ and $g_{\eta_X\gamma V}$. For the kinematics near the pole masses of η_X, this approximation is reasonable. The decay coupling $g_{\eta_X\gamma V}$ contains contributions from both tree-level and loop amplitudes, i.e., $g_{\eta_X\gamma V} = g^T_{\eta_X\gamma V} + g^L_{\eta_X\gamma V}$ with the superscripts T and L indicating the tree and loop processes, respectively. These two quantities, $g^T_{\eta_X\gamma V}$ and $g^L_{\eta_X\gamma V}$, will then be calculated in our model.

B. Tree-level amplitude in the VMD model

In this work, we adopt the VMD model [46] to describe the EM vertices. With the Lagrangian of Eq. (5) and the VMD model, the amplitude of the tree diagram shown in Fig. 1(a) can be written as

$$i\mathcal{M}_T = i g^T_{\eta_X\gamma V}\epsilon_{\alpha\beta\delta\lambda} p^\alpha_\gamma p^\beta_V \epsilon^\delta_\gamma \epsilon^\lambda_V, \quad (8)$$

where the tree-level effective coupling $g^T_{\eta_X\gamma V}$ can be expressed as

$$g^T_{\eta_X\gamma V} \equiv -i g_{\eta_X VV}\frac{e m_V^2}{f_V} G_V, \quad (9)$$

where G_V is the propagator of the intermediate vector meson V,

$$G_V \equiv \frac{-i}{p^2_\gamma - m^2_V + i m_V \Gamma_V}, \quad (10)$$

with V denoting the vector meson ρ^0, ω, or ϕ, which is the same as the final-state vector meson in $\eta_X \to \gamma V$ as required by the isospin symmetry. The strong coupling constants $g_{\eta_X VV}$ can be extracted by other independent processes. Then, the couplings for other vectors within the same SU(3) multiplet can be related to each other by the SU(3) symmetry. We will come back to this in the next subsection with detailed extraction of $g_{\eta_X VV}$.

The vector meson decay constant e/f_V can be determined by $V \to e^+e^-$ using the experimental data, which can be expressed as

$$\frac{e}{f_V} = \left(\frac{3\Gamma_{V\to e^+e^-}}{2\alpha_e |\mathbf{p}_e|}\right)^{1/2}, \quad (11)$$

where $\mathbf{p}_e$ is the three-vector momentum of the electron in the vector-meson rest frame. The values for different vector meson decays are extracted by adopting the experimental data of the vector meson decays into e^+e^- [1], and they are listed in Table II.

C. Loop amplitudes in the VMD model

1. Lagrangians and coupling constants

The triangle loop amplitudes illustrated by Fig. 1(b) can also be calculated in the VMD model. The loop amplitudes can reduce to an effective coupling which contributes to the $\eta_X\gamma V$ coupling in the end. Within the triangle loops, the vertices for the photon couplings to the kaon and/or K^* pairs can be described by the VMD model. Taking the $K^{*+}K^-$ coupling to the photon γ as an example, the photon can couple to the intermediate ρ^0, ω, and ϕ mesons, via the following amplitude,

$$g_{K^{*+}K^-\gamma} = \sum_{q=u,s}\sum_{V=\rho,\omega,\phi}\langle (q\bar{q})_{1^{--}}|V\rangle i g_{V'VP}\frac{e m_V^2}{f_V} G_V, \quad (12)$$

where V' and P stand for the initial K^{*+} and pseudoscalar meson K^-, while V stands for the intermediate vector mesons, ρ^0, ω, and ϕ, to which the photon can couple with a strength of the decay constant e/f_V; $\langle (q\bar{q})_{1^{--}}|V\rangle$ is a favor factor given by the decomposition of the $q\bar{q}$ into flavor eigenstate of the intermediate vector mesons. For instance, we have

$$\langle (u\bar{u})_{1^{--}}|V\rangle = \left\langle \left[\frac{1}{2}(u\bar{u}-d\bar{d})+\frac{1}{2}(u\bar{u}+d\bar{d})\right]|V\rangle, \right.$$
$$= \frac{1}{\sqrt{2}}\langle(\rho^0+\omega)|V\rangle. \quad (13)$$

For each transition, we present the detailed expressions as

$$g_{K^{*+}K^-\gamma} = \frac{i}{\sqrt{2}}\left(g_{\omega K^{*+}K^-}\frac{em_\omega^2}{f_\omega}G_\omega + g_{\rho K^{*+}K^-}\frac{em_\rho^2}{f_\rho}G_\rho\right) + ig_{\phi K^{*+}K^-}\frac{em_\phi^2}{f_\phi}RG_\phi, \quad (14)$$

$$g_{K^{*0}\bar{K}^0\gamma} = \frac{i}{\sqrt{2}}\left(g_{\omega K^{*0}\bar{K}^0}\frac{em_\omega^2}{f_\omega}G_\omega + g_{\rho K^{*0}\bar{K}^0}\frac{em_\rho^2}{f_\rho}G_\rho\right) + ig_{\phi K^{*0}\bar{K}^0}\frac{em_\phi^2}{f_\phi}RG_\phi \quad (15)$$

for the $K^*K\gamma$ vertex,

$$g_{K^{*+}K^{*-}\gamma} = \frac{i}{\sqrt{2}}\left(g_{\omega K^{*+}K^{*-}}\frac{em_\omega^2}{f_\omega}G_\omega + g_{\rho K^{*+}K^{*-}}\frac{em_\rho^2}{f_\rho}G_\rho\right) + ig_{\phi K^{*+}K^{*-}}\frac{em_\phi^2}{f_\phi}RG_\phi, \quad (16)$$

$$g_{K^{*0}\bar{K}^{*0}\gamma} = \frac{i}{\sqrt{2}}\left(g_{\omega K^{*0}\bar{K}^{*0}}\frac{em_\omega^2}{f_\omega}G_\omega + g_{\rho K^{*0}\bar{K}^{*0}}\frac{em_\rho^2}{f_\rho}G_\rho\right) + ig_{\phi K^{*0}\bar{K}^{*0}}\frac{em_\phi^2}{f_\phi}RG_\phi \quad (17)$$

for the $K^*\bar{K}^*\gamma$ vertex, and

$$g_{K^+K^-\gamma} = \frac{i}{\sqrt{2}}\left(g_{\omega K^+K^-}\frac{em_\omega^2}{f_\omega}G_\omega + g_{\rho K^+K^-}\frac{em_\rho^2}{f_\rho}G_\rho\right) + ig_{\phi K^+K^-}\frac{em_\phi^2}{f_\phi}RG_\phi, \quad (18)$$

$$g_{K^0\bar{K}^0\gamma} = \frac{i}{\sqrt{2}}\left(g_{\omega K^0\bar{K}^0}\frac{em_\omega^2}{f_\omega}G_\omega + g_{\rho K^0\bar{K}^0}\frac{em_\rho^2}{f_\rho}G_\rho\right) + ig_{\phi K^0\bar{K}^0}\frac{em_\phi^2}{f_\phi}RG_\phi \quad (19)$$

for the $K\bar{K}\gamma$ vertex. The ground-state vector meson decay constants e/f_V ($V=\phi,\rho^0,\omega$) have been given by Eq. (11), and their values are listed in Table II.

TABLE II. Vector meson decay constants determined by $V\to e^+e^-$. The data are taken from the PDG [1].

Channel	Total width of V	BR($V\to e^+e^-$)	$e/f_V(\times10^{-2})$
$\phi\to e^+e^-$	4.25 MeV	$(2.97\pm0.04)\times10^{-4}$	−2.26
$\rho^0\to e^+e^-$	147.8 MeV	$(4.72\pm0.05)\times10^{-5}$	6.05
$\omega\to e^+e^-$	8.49 MeV	$(7.36\pm0.15)\times10^{-5}$	1.78

For the hadronic vertices, one can see that they can be arranged by the SU(3) symmetry. Thus, their relative strengths and phases are fixed. There are three types of hadronic coupling vertices in the loop amplitudes, i.e., VPP, VVP, and VVV, for which effective Lagrangians are adopted. The corresponding effective Lagrangians are

$$\mathcal{L}_{VPP} = ig_{VPP}\mathrm{Tr}[(P\partial_\mu P-\partial_\mu PP)V^\mu], \quad (20)$$

$$\mathcal{L}_{VVP} = g_{VVP}\epsilon_{\alpha\beta\mu\nu}\mathrm{Tr}[\partial^\alpha V^\mu\partial^\beta V^\nu P], \quad (21)$$

$$\mathcal{L}_{VVV} = ig_{VVV}\langle(\partial_\mu V_\nu-\partial_\nu V_\mu)V^\mu V^\nu\rangle, \quad (22)$$

where V and P stand for the vector and pseudoscalar fields for the flavor SU(3) multiplets, respectively, and they have the forms

$$P = \begin{pmatrix} \frac{\sin\alpha_P\eta'+\cos\alpha_P\eta+\pi^0}{\sqrt{2}} & \pi^+ & K^+ \\ \pi^- & \frac{\sin\alpha_P\eta'+\cos\alpha_P\eta-\pi^0}{\sqrt{2}} & K^0 \\ K^- & \bar{K}^0 & \cos\alpha_P\eta'-\sin\alpha_P\eta \end{pmatrix} \quad (23)$$

and

$$V = \begin{pmatrix} \frac{\omega+\rho^0}{\sqrt{2}} & \rho^+ & K^{*+} \\ \rho^- & \frac{\omega-\rho^0}{\sqrt{2}} & K^{*0} \\ K^{*-} & \bar{K}^{*0} & \phi \end{pmatrix}, \quad (24)$$

where the ideal mixing between ω ($=(u\bar{u}+d\bar{d})/\sqrt{2}$) and ϕ ($=s\bar{s}$) is implied.

Note that we adopt the same form as Eq. (23) for the first radial excitation states of the pseudoscalar mesons.

Considering the η_X coupling to $K^*\bar{K}$, the effective Lagrangians have the expressions

$$\mathcal{L}_{\eta(1405)K^{*+}K^-} = ig_{\eta(1405)K^{*+}K^-}(K^-\partial_\mu\eta(1405)-\eta(1405)\partial_\mu K^-)(K^{*+})^\mu \equiv ig_{XVP}\left(\frac{\sin\alpha_P}{\sqrt{2}}R-\cos\alpha_P\right)(K^-\partial_\mu\eta(1405)-\eta(1405)\partial_\mu K^-)(K^{*+})^\mu, \quad (25)$$

and

$$\mathcal{L}_{\eta(1295)K^{*+}K^-} = ig_{\eta(1295)K^{*+}K^-}(K^-\partial_\mu\eta(1295) - \eta(1295)\partial_\mu K^-)(K^{*+})^\mu$$
$$\equiv ig_{XVP}\left(\frac{\cos\alpha_P}{\sqrt{2}}R + \sin\alpha_P\right)(K^-\partial_\mu\eta(1295) - \eta(1295)\partial_\mu K^-)(K^{*+})^\mu, \quad (26)$$

where g_{XVP} is the overall coupling between a radial excitation pseudoscalar $q\bar{q}$ and $K^{*+}K^-$ and will be determined later; R is the SU(3) flavor symmetry-breaking factor defined earlier.

Couplings between η_X and $K^*\bar{K}^*$ also contribute to the loop amplitudes. The corresponding Lagrangians are

$$\mathcal{L}_{\eta(1405)K^{*+}K^{*-}} = g_{XVV}\epsilon_{\alpha\beta\mu\nu}\left[\frac{\sin\alpha_P}{\sqrt{2}}R\partial^\alpha(K^{*+})^\mu\partial^\beta(K^{*-})^\nu\eta(1405) + \cos\alpha_P\partial^\alpha(K^{*-})^\mu\partial^\beta(K^{*+})^\nu\eta(1405)\right]$$
$$= g_{XVV}\left(\frac{\sin\alpha_P}{\sqrt{2}}R + \cos\alpha_P\right)\epsilon_{\alpha\beta\mu\nu}\partial^\alpha(K^{*+})^\mu\partial^\beta(K^{*-})^\nu\eta(1405) \quad (27)$$

for the $\eta(1405)K^{*+}K^{*-}$ coupling and

$$\mathcal{L}_{\eta(1295)K^{*+}K^{*-}} = g_{XVV}\left(\frac{\cos\alpha_P}{\sqrt{2}}R - \sin\alpha_P\right)\epsilon_{\alpha\beta\mu\nu}$$
$$\times\partial^\alpha(K^{*+})^\mu\partial^\beta(K^{*-})^\nu\eta(1295) \quad (28)$$

for the $\eta(1295)K^{*+}K^{*-}$ coupling, respectively. The coupling g_{XVV} is the overall coupling strength of the first radial excitation state of a $(q\bar{q})_{0^{-+}}$ to a vector meson pair. This quantity will be determined by the combined analysis of the data for $J/\psi \to \gamma\eta(1405/1475) \to \gamma K\bar{K}\pi$ and $J/\psi \to \gamma\eta(1405/1475) \to \gamma\gamma\rho^0$ [1].

The other hadronic vertices, which involve the interactions between the ground-state vector and pseudoscalar mesons, can be obtained by expanding Eqs. (20)–(22).

We adopt the following strategy to determine the coupling constants:

(i) In our calculation, we take the same sign for the ground-state coupling g_{VPP} and g_{XVP}. They are defined as positive and real numbers, and then the signs for the other couplings will be fixed.

(ii) The coupling g_{VPP} between the ground-state vector and pseudoscalar mesons can be determined by $\phi \to K^+K^-$. Then, the other VPP couplings can be related to $g_{\phi K^+K^-}$ by the SU(3) flavor symmetry. We note that one can also extract g_{VPP} via $\rho \to \pi\pi$, and some SU(3) flavor symmetry-breaking effects can be found. By adopting the coupling extracted from $\phi \to K\bar{K}$, we actually absorb some leading SU(3) flavor symmetry-breaking effects into this quantity since all the vertices in the loop processes involve couplings with the strange mesons. The corresponding couplings $g_{\phi K^+K^-}$ and g_{VPP} are listed in Table III.

(iii) The coupling g_{VVP} in the loop between the ground-state vector and pseudoscalar mesons is determined by fitting the experimental data for $V \to \gamma P$ and $\eta' \to \gamma V$ in the VMD model. For these transitions between the ground-state vector and pseudoscalar mesons, we assume that the intermediate ground-state vector mesons saturate the transition amplitudes. The corresponding channels and fitting results are listed in Table IV, and the best fitting gives $g_{VVP} = 8.38 \pm 0.1\ \text{GeV}^{-1}$. We then adopt $g_{VVP} = 8.38\ \text{GeV}^{-1}$ to extract other VVP couplings in the loop amplitudes which are listed in Table V. The sign is determined to be consistent with the g_{VPP} following the $^3P_0$ model.

TABLE III. Strong couplings adopted for the VPP vertices in the $K^*\bar{K}(K^{(*)})$ loops.

VPP coupling constant	Values
$g_{\phi K^+K^-}$	4.47
$g_{\rho K^+K^-}$	$-\frac{g_{\phi K^+K^-}}{\sqrt{2}}$
$g_{\omega K^+K^-}$	$-\frac{g_{\phi K^+K^-}}{\sqrt{2}}$
g_{VPP}	4.47

TABLE IV. The fitted radiative transitions between the ground-state vector and pseudoscalar mesons in comparison with the experimental data in the VMD model. The best fitting gives $g_{VVP} = 8.38 \pm 0.1\ \text{GeV}^{-1}$.

Channels	Experiments (MeV)	Fitted values (MeV)
$\eta' \to \gamma\rho$	$(6.7 \pm 0.7) \times 10^{-2}$	$(8.6 \pm 0.2) \times 10^{-2}$
$\rho \to \gamma\eta$	$(4.5 \pm 0.3) \times 10^{-2}$	$(5 \pm 0.1) \times 10^{-2}$
$\rho \to \gamma\pi$	$(7 \pm 1) \times 10^{-2}$	$(6.1 \pm 0.1) \times 10^{-2}$
$\eta' \to \gamma\omega$	$(5.8 \pm 0.7) \times 10^{-3}$	$(6.4 \pm 0.2) \times 10^{-3}$
$\omega \to \gamma\eta$	$(3.8 \pm 0.4) \times 10^{-3}$	$(5.2 \pm 0.1) \times 10^{-3}$
$\omega \to \gamma\pi$	0.71 ± 0.03	0.72 ± 0.02
$\phi \to \gamma\eta'$	$(2.6 \pm 0.1) \times 10^{-4}$	$(2.9 \pm 0.1) \times 10^{-4}$
$\phi \to \gamma\eta$	$(5.5 \pm 0.1) \times 10^{-2}$	$(5.2 \pm 0.1) \times 10^{-2}$
$K^{*\pm} \to \gamma K^\pm$	$(5 \pm 0.5) \times 10^{-2}$	$(2.4 \pm 0.05) \times 10^{-2}$
$K^{*0}(\bar{K}^{*0}) \to \gamma K^0(\bar{K}^0)$	0.12 ± 0.01	0.081 ± 0.002

TABLE V. Strong couplings adopted for the vertices in the $K^*\bar{K}(K^{(*)})$ loops.

VVP	Values (GeV^{-1})	VVV	Values
$g_{\phi K^{*+}K^-}$	8.38	$g_{\phi K^{*+}K^{*-}}$	4.47
$g_{\rho K^{*+}K^-}$	$\frac{g_{\phi K^{*+}K^-}}{\sqrt{2}}$	$g_{\rho K^{*+}K^{*-}}$	$-\frac{g_{\phi K^{*+}K^{*-}}}{\sqrt{2}}$
$g_{\omega K^{*+}K^-}$	$\frac{g_{\phi K^{*+}K^-}}{\sqrt{2}}$	$g_{\omega K^{*+}K^{*-}}$	$-\frac{g_{\phi K^{*+}K^{*-}}}{\sqrt{2}}$
g_{VVP}	8.38	g_{VVV}	4.47

(iv) The strong couplings g_{VVV}, g_{VVP}, and g_{VPP} can be related to each other by matching the relation of their corresponding transition amplitudes in an effective Lagrangian approach (ELA) to the same relation which can be extracted explicitly in the quark pair creation (QPC) model (i.e., $^3P_0$ model). In Appendix B, we provide the main formalisms for the QPC model calculations as a reference. The values of g_{VVV} for the relevant channels are also listed in Table V. We mention that the two couplings g_{VPP} and g_{VVP} hold a reasonable relation to that extracted in the quark model, i.e., $g_{VPP} \simeq m_V g_{VVP}/2$.

(v) The physical coupling $g_{\eta(1405)K^*\bar{K}}$ can be extracted from experimental data by a combined analysis of the $\eta(1405)$ decays into $K\bar{K}\pi$, $\eta\pi\pi$, and 3π [34,37]. By adopting the branching ratio $B.R.(\eta(1405) \to K^*\bar{K} + \text{c.c.}) \simeq 50\%$ and the total width $\Gamma_{\eta(1405)} = 90$ MeV, we can extract g_{XVP} with $\alpha_P = 42°$ [37]. Then, both $g_{\eta(1405)K^{*+}K^-}$ and $g_{\eta(1295)K^{*+}K^-}$ can be determined. Their values are listed in Table VI. The overall coupling g_{XVP} can also be determined. The extracted values are listed in Table VI.

(vi) One can determine g_{XVV} by matching the partial decay width of $\eta(1405) \to \gamma\rho^0$ to the existing data [47]. We will show later that the g_{XVV} determined in this way is reasonable since the decay width for $\eta(1405) \to \gamma\rho$ is dominated by the tree-level transition amplitude and the loop contributions are negligibly small. Then, by taking the ratio of $\mathrm{BR}(J/\psi \to \gamma\eta(1405) \to \gamma\gamma\rho^0)/\mathrm{BR}(J/\psi \to \gamma\eta(1405) \to \gamma K^*\bar{K} + \text{c.c.})$ and with the constraint from the experimental data (see Table I and Refs. [41,45]), we can extract $g_{XVV} = 9.5 \pm 1.5$ as listed in Table VII.

TABLE VI. Hadronic couplings for $\eta_X \to K^{*+}K^-$ based on $g_{\eta(1405)K^{*+}K^-} = -3.64$ determined by combined analyses of the decays of $\eta(1405) \to K^*\bar{K} + \text{c.c.}$ and $\eta\pi\pi$ [34,37]. $\alpha_P = 42°$ is adopted for the mixing between $\eta(1295)$ and $\eta(1405)$.

$\eta_X VP$	Values
$g_{\eta(1405)K^{*+}K^-}$	-3.64 [34,37]
$g_{\eta(1295)K^{*+}K^-}$	10.9
g_{XVP}	9.98

TABLE VII. Strong couplings for $\eta_X \to VV$ in the VMD model. The overall coupling $g_{XVV} = 9.5 \pm 1.5$ is extracted by the combined analysis of $J/\psi \to \gamma\eta(1405) \to \gamma\gamma\rho^0$ and $J/\psi \to \gamma\eta(1405) \to \gamma K^*\bar{K} + \text{c.c.}$ We adopt the central value of $g_{XVV} = 9.5$ in the numerical calculation.

Coupling constant	Expression	Value (GeV^{-1})
$g_{\eta(1295)K^{*+}K^{*-}}$	$g_{XVV}(R\cos\alpha_P/\sqrt{2} - \sin\alpha_P)$	-1.36 ± 0.22
$g_{\eta(1405)K^{*+}K^{*-}}$	$g_{XVV}(R\sin\alpha_P/\sqrt{2} + \cos\alpha_P)$	11.6 ± 1.8
$g_{\eta(1295)\rho\rho}$	$\sqrt{2}g_{XVV}\cos\alpha_P$	10.0 ± 1.6
$g_{\eta(1405)\rho\rho}$	$\sqrt{2}g_{XVV}\sin\alpha_P$	9.0 ± 1.4
$g_{\eta(1295)\omega\omega}$	$\sqrt{2}g_{XVV}\cos\alpha_P$	10.0 ± 1.6
$g_{\eta(1405)\omega\omega}$	$\sqrt{2}g_{XVV}\sin\alpha_P$	9.0 ± 1.4
$g_{\eta(1295)\phi\phi}$	$-2g_{XVV}R\sin\alpha_P$	-10.2 ± 1.6
$g_{\eta(1405)\phi\phi}$	$2g_{XVV}R\cos\alpha_P$	11.3 ± 1.8
g_{XVV}	…	9.5 ± 1.5

TABLE VIII. The effective couplings for the $K^*K^{(*)}\gamma$ transitions. The values extracted from the VMD model are listed in the second column, and their corresponding modules are presented in the parentheses. In the last column, the signs of the $g_{K^*K\gamma}$ couplings are determined in the quark model. The couplings $g_{K^*K^*\gamma}$ and $g_{KK\gamma}$ are treated as pure QED couplings. Thus, their coupling strengths will be given by the charge of the hadron. Note that $e \simeq 0.3$.

Electromagnetic couplings	Values in VMD (magnitude)	Experimental values
$g_{K^{*+}K^+\gamma}$ (GeV^{-1})	$-0.17 - i0.05$ (0.18)	-0.25
$g_{K^{*0}K^0\gamma}$ (GeV^{-1})	$0.33 + 0.05i$ (0.33)	0.38
$g_{K^{*+}K^{*+}\gamma}$	$0.25 + 0.026i$ (0.25)	e
$g_{K^{*0}K^{*0}\gamma}$	$-0.01 - 0.024i$ (0.03)	0
$g_{K^+K^+\gamma}$	$0.25 + 0.026i$ (0.25)	e
$g_{K^0K^0\gamma}$	$-0.01 - 0.024i$ (0.03)	0

Combining the couplings collected in Tables II and V, we can extract the effective couplings defined in Eqs. (14)–(19) as a test of the VMD model, and the couplings are listed in Table VIII. Since the widths of the intermediate vector mesons are considered, the couplings extracted in the VMD are complex numbers. In Table VIII, we also provide the magnitudes of the complex couplings in round brackets in order to compare with the quantities extracted from experiment. One can see that the VMD model has accounted for the experimental data reasonably well under the assumption of the ground-state vector meson saturation.

The relations for couplings among the flavor SU(3) multiplets will be explicitly presented in the construction of each loop amplitude.

2. Loop amplitudes

With the above effective Lagrangians, we can write down the loop transition amplitudes for Figs. 1(b)–1(d). For

the triangle loops [Fig. 1(b)], we use the notation $[M1, M3, (M2)]$ to denote the intermediate interaction between particle $M1$ and $M3$ by exchanging $M2$; e.g., $[K^*, \bar{K}, (K)]$ represents the loop where the intermediate K^* and $\bar{K}$ scatter into the final states by exchanging K. The masses and 4-vector momenta of these internal particles are denoted by (m_1, m_3, m_2) and (p_1, p_3, p_2), respectively. The 4-vector momenta of the initial-state meson X, final-state photon, and vector meson are labeled as p_X, p_γ, and p_V, respectively. The polarizations of the final-state photon and vector meson are ϵ_γ and ϵ_V, respectively. Similarly, we adopt notation $[M1, M2]$ for the internal mesons in Figs. 1(c)–1(d).

To cut off the UV divergence in the loop integrals, we include a commonly adopted form factor to regularize the integrand,

$$\mathcal{F}(\boldsymbol{p}_i^2) = \prod_i \exp\left(-\frac{\boldsymbol{p}_i^2}{\Lambda^2}\right), \tag{29}$$

where Λ is the cutoff energy and its typical value is around the ρ mass; $\boldsymbol{p}_i$ is the 3-momentum of the ith particle in the loops in the c.m. frame of the initial particle. In the loop integrals, we first reduce the four-dimension integrations into the three-dimension ones by integrating the energy component and then regularize the integrands by the above form factor. Such a form factor originates from the quark model wave function convolutions at the coupling vertices. The corresponding hadronic coupling constant is usually defined with all the interacting hadrons being at rest. For instance, in a decay process where the final-state hadrons carry momenta, suppressions or corrections to the constant coupling will be introduced by the wave function convolutions which have a form as Eq. (29).

As follows, we will write down the detailed amplitude for each loop transition with explicit phase conventions.

$[K^*, \bar{K}, (K)]$.—The amplitude for the $[K^*, \bar{K}, (K)]$ loop is

$$i\mathcal{M} = \int \frac{d^4p_1}{(2\pi)^4} V_{1\sigma} D^{\sigma\mu}(K^*) V_{2\mu} V_3 D(K) D(\bar{K}) \mathcal{F}(\boldsymbol{p}_i^2), \tag{30}$$

where the vertex functions have been expressed by a compact form and have the expressions

$$\begin{aligned} V_{1\sigma} &= i g_{\eta_X K^* \bar{K}} (p_X + p_3)_\sigma, \\ V_{2\mu} &= i g_{K^* K\gamma} \epsilon_{\alpha\beta\delta\mu} p_\gamma^\alpha p_1^\beta \epsilon_\gamma^\delta, \\ V_3 &= iR g_{VK\bar{K}} (p_2 - p_3)_\lambda \epsilon_V^\lambda, \end{aligned} \tag{31}$$

with the SU(3) flavor symmetry-breaking factor R included if the interacting vector meson $V = \rho$ and ω. In Eq. (30), functions $D^{\sigma\mu}(K^*)$ and $D(K)$ are the propagators for K^* and K, respectively, with 4-vector momentum p, i.e.,

$$\begin{aligned} D^{\sigma\mu}(K^*) &= \frac{-i(g^{\sigma\mu} - \frac{p^\sigma p^\mu}{p^2})}{p^2 - m_{K^*}^2 + i\epsilon} \\ D(K) &= \frac{i}{p^2 - m_K^2 + i\epsilon}. \end{aligned} \tag{32}$$

In the calculations, the propagators will carry the corresponding 4-vector momenta required by momentum conservation.

There are four isospin channels for this type of triangle diagram, which include $[K^{*+}, K^+, (K^-)]$, $[K^{*-}, K^-, (K^+)]$, $[K^{*0}, K^0, (\bar{K}^0)]$, and $[\bar{K}^{*0}, \bar{K}^0(K^0)]$. The vertex coupling constants are connected by the SU(3) flavor symmetry:

$$\begin{aligned} g_{\eta_X K^{*+} K^-} &= -g_{\eta_X K^{*-} K^+} = g_{\eta_X K^{*0} \bar{K}^0} = -g_{\eta_X \bar{K}^{*0} K^0}, \\ g_{\phi K^+ K^-} &= -g_{\phi K^- K^+} = g_{\phi K^0 \bar{K}^0} = -g_{\phi \bar{K}^0 K^0}, \\ g_{\omega K^+ K^-} &= -g_{\omega K^- K^+} = g_{\omega K^0 \bar{K}^0} = -g_{\omega \bar{K}^0 K^0}, \\ g_{\rho K^+ K^-} &= -g_{\rho K^- K^+} = -g_{\rho K^0 \bar{K}^0} = g_{\rho \bar{K}^0 K^0}. \end{aligned} \tag{33}$$

The coupling constants for the sum of all the isospin channels of the $[K^*, \bar{K}, (K)]$ loop can be written as the following forms for the $\gamma\phi$, $\gamma\omega$, and $\gamma\rho$ channels, respectively:

$$2 g_{\eta_X K^{*+} K^-} g_{\phi K^+ K^-} (g_{K^{*+} K^+ \gamma} + g_{K^{*0} K^0 \gamma}), \tag{34}$$

$$2 g_{\eta_X K^{*+} K^-} g_{\omega K^+ K^-} (g_{K^{*+} K^+ \gamma} + g_{K^{*0} K^0 \gamma}), \tag{35}$$

$$2 g_{\eta_X K^{*+} K^-} g_{\rho K^+ K^-} (g_{K^{*+} K^+ \gamma} - g_{K^{*0} K^0 \gamma}). \tag{36}$$

As listed in Table VIII, the couplings $g_{K^{*+} K^+ \gamma}$ and $g_{K^{*0} K^0 \gamma}$ have a sign phase, which implies the constructive phase between the charged and neutral meson loops for $\eta_X \to \gamma\rho$, while the $\gamma\phi$ and $\gamma\omega$ channels involve a destructive phase.

The loop integral will be given in the Appendix, and the contributions of each type of the loop transitions will be collected and compared with each other among different processes.

$[K^*, \bar{K}, (K^*)]$.—Similarly, by denoting the masses and 4-vector momenta of the intermediate mesons $(K^*, K^*, \bar{K})$ as (m_1, m_2, m_3) and (p_1, p_2, p_3), respectively, the loop transition amplitude can be written as

$$i\mathcal{M} = \int \frac{d^4p_1}{(2\pi)^4} V_{1\sigma} D^{\sigma\mu}(K^*) V_{2\mu\rho} D^{\rho\nu}(K^*) V_{3\nu} D(\bar{K}) \mathcal{F}(\boldsymbol{p}_i^2), \tag{37}$$

where the vertex function $V_{1\sigma}$ has the same form as that in Eq. (31) and the other two functions are

$$V_{2\mu\rho} = -ig_{K^*K^*\gamma}[\epsilon_\gamma^\delta g_{\delta\mu} p_{1\rho} + \epsilon_\gamma^\delta g_{\delta\rho} p_{2\mu} - g_{\mu\rho}(p_1 + p_2)_\delta \epsilon_\gamma^\delta], \tag{38}$$

$$V_{3\nu} = iRg_{VK^{*+}K^-}\epsilon_{\alpha\beta\nu\lambda} p_2^\alpha p_V^\beta \epsilon_V^\lambda. \tag{39}$$

Similar to the previous loop amplitude, there are also four isospin channels which involve the charged and neutral intermediate mesons. They can be combined together with the coupling constants for the $\gamma\phi$, $\gamma\omega$, and $\gamma\rho^0$ channels, respectively, i.e.,

$$2g_{\eta_\chi K^{*+}K^-} g_{\phi K^{*+}K^-}(g_{K^{*+}K^{*+}\gamma} + g_{K^{*0}K^{*0}\gamma}), \tag{40}$$

$$2g_{\eta_\chi K^{*+}K^-} g_{\omega K^{*+}K^-}(g_{K^{*+}K^{*+}\gamma} + g_{K^{*0}K^{*0}\gamma}), \tag{41}$$

$$2g_{\eta_\chi K^{*+}K^-} g_{\rho K^{*+}K^-}(g_{K^{*+}K^{*+}\gamma} - g_{K^{*0}K^{*0}\gamma}). \tag{42}$$

As listed in Table VIII, the charge neutral coupling $g_{K^{*0}K^{*0}\gamma}$ is much smaller than the charged one.

$[K^*, \bar{K}^*, (K)]$.—With the same notation convention for the masses and 4-vector momenta of the intermediate mesons, the loop amplitude can be expressed as

$$i\mathcal{M} = \int \frac{d^4 p_1}{(2\pi)^4} V_{1\mu\nu} D^{\mu\mu'}(K*) V_{2\mu'} D(K) V_{3\nu'} D^{\nu'\nu}(\bar{K}^*) \mathcal{F}(\boldsymbol{p}_i^2), \tag{43}$$

where the vertex function $V_{2\mu'}$ has been given in Eq. (31) and the other two vertex functions are

$$V_{1\mu\nu} = -ig_{\eta_\chi K^* \bar{K}^*}\epsilon_{\alpha\beta\mu\nu} p_1^\alpha p_3^\beta \tag{44}$$

$$V_{3\nu'} = iRg_{VK^*\bar{K}}\epsilon_{\alpha_2\beta_2\nu'\lambda} p_3^{\alpha_2} p_V^{\beta_2} \epsilon_V^\lambda. \tag{45}$$

Combining together the four isospin channels, we have the coupling constants for the $\gamma\phi$, $\gamma\omega$, and $\gamma\rho^0$ decays, respectively, as follows:

$$2g_{\eta_\chi K^{*+}K^{*-}} g_{\phi K^{*+}K^-}(g_{K^{*+}K^+\gamma} + g_{K^{*0}K^0\gamma}), \tag{46}$$

$$2g_{\eta_\chi K^{*+}K^{*-}} g_{\omega K^{*+}K^-}(g_{K^{*+}K^+\gamma} + g_{K^{*0}K^0\gamma}), \tag{47}$$

$$2g_{\eta_\chi K^{*+}K^{*-}} g_{\rho K^{*+}K^-}(g_{K^{*+}K^+\gamma} - g_{K^{*0}K^0\gamma}). \tag{48}$$

$[K^*, \bar{K}^*, (K^*)]$.—The transition amplitude can be written as

$$i\mathcal{M} = \int \frac{d^4 p_1}{(2\pi)^4} V_{1\mu\nu} D^{\mu\mu'}(K^*) V_{2\mu'\rho} D^{\rho\sigma}(K^*) V_{3\nu'\sigma} \times D^{\nu'\nu}(\bar{K}^*) \mathcal{F}(\boldsymbol{p}_i^2), \tag{49}$$

where the vertex functions have been given earlier for the corresponding couplings. Similar to the loop amplitudes discussed, we combine the isospin channels together to give the couplings for the $\gamma\phi$, $\gamma\omega$, and $\gamma\rho^0$ decays, respectively, as follows:

$$2g_{\eta_\chi K^{*+}K^{*-}} g_{\phi K^{*+}K^{*-}}(g_{K^{*+}K^{*+}\gamma} + g_{K^{*0}K^{*0}\gamma}), \tag{50}$$

$$2g_{\eta_\chi K^{*+}K^{*-}} g_{\omega K^{*+}K^{*-}}(g_{K^{*+}K^{*+}\gamma} + g_{K^{*0}K^{*0}\gamma}), \tag{51}$$

$$2g_{\eta_\chi K^{*+}K^{*-}} g_{\rho K^{*+}K^{*-}}(g_{K^{*+}K^{*+}\gamma} - g_{K^{*0}K^{*0}\gamma}). \tag{52}$$

$[K, \bar{K}^*, (K)]$.—The transition amplitude can be written as

$$i\mathcal{M} = \int \frac{d^4 p_1}{(2\pi)^4} V_{1\mu} D(K) V_2 D(K) V_{3\nu} D^{\mu\nu}(\bar{K}^*) \mathcal{F}(\boldsymbol{p}_i^2), \tag{53}$$

where the vertex functions $V_{1\mu}$ and $V_{3\nu}$ have been given earlier and V_2 has the following form:

$$V_2 = ig_{KK\gamma}(p_1 + p_2)_\delta \epsilon_\gamma^\delta. \tag{54}$$

Again, combining the four isospin channels of this type of the loop transitions, we obtain the coupling constants for the $\gamma\phi$, $\gamma\omega$, and $\gamma\rho^0$ decays, respectively, as

$$2g_{\eta_\chi K^+K^{*-}} g_{\phi K^+K^{*-}}(g_{K^+K^+\gamma} + g_{K^0K^0\gamma}), \tag{55}$$

$$2g_{\eta_\chi K^+K^{*-}} g_{\omega K^+K^{*-}}(g_{K^+K^+\gamma} + g_{K^0K^0\gamma}), \tag{56}$$

$$2g_{\eta_\chi K^+K^{*-}} g_{\rho K^+K^{*-}}(g_{K^+K^+\gamma} - g_{K^0K^0\gamma}), \tag{57}$$

where the charge neutral amplitudes vanish literally due to the suppressed coupling $g_{K^0K^0\gamma}$.

$[K, \bar{K}^*, (K^*)]$.—The transition amplitude can be written as

$$i\mathcal{M} = \int \frac{d^4 p_1}{(2\pi)^4} V_{1\mu} D(K) V_{2\nu} D^{\nu\nu'}(K^*) V_{3\mu'\nu'} D^{\mu\mu'}(\bar{K}^*) \mathcal{F}(\boldsymbol{p}_i^2), \tag{58}$$

where all the vertex functions have been given earlier. The combined couplings for these four isospin channels can be expressed as the following forms for the $\gamma\phi$, $\gamma\omega$, and $\gamma\rho^0$ decays, respectively:

$$2g_{\eta_\chi K^+K^{*-}} g_{\phi K^{*+}K^{*-}}(g_{K^{*+}K^+\gamma} + g_{K^{*0}K^0\gamma}), \tag{59}$$

$$2g_{\eta_\chi K^+K^{*-}} g_{\omega K^{*+}K^{*-}}(g_{K^{*+}K^+\gamma} + g_{K^{*0}K^0\gamma}), \tag{60}$$

$$2g_{\eta_\chi K^+K^{*-}} g_{\rho K^{*+}K^{*-}}(g_{K^{*+}K^+\gamma} - g_{K^{*0}K^0\gamma}). \tag{61}$$

Contact loop diagrams.—Besides the triangle loop transitions, the photon can be produced by the minimum

substitution of the derivative at the hadronic interaction vertices, i.e.,

$$\partial_\mu \to \partial_\mu + ie\hat{Q}A_\mu. \tag{62}$$

Such contributions are illustrated by Figs. 1(c) and 1(d) and are referred to as the contact loop diagrams in this paper.

For Figs. 1(c) or 1(d), the intermediate mesons $[M1, M2]$ both could be $[K^*, \bar{K}]$ or $[K^*, \bar{K}^*]$. It can be easily proven that contributions from Fig. 1(c) with either $[K^*, \bar{K}]$ or $[K^*, \bar{K}^*]$ should vanish [48]. For Fig. 1(d) with $[M1, M2] = [K^*, \bar{K}^*]$, the antisymmetric tensor coupling for the $\eta_X K^* \bar{K}^*$ vertex dictates that the induced photon can only contribute via its longitudinal component. Thus, for the real photon decay, this transition will be forbidden. As a result, only the transition of Fig. 1(d) with the intermediate $K^*\bar{K}$ mesons will have nonvanishing contributions, and the corresponding amplitude can be expressed as

$$i\mathcal{M} = \int \frac{d^4p_1}{(2\pi)^4} V_{1\mu} D^{\mu\alpha}(K^{*+}) V_{2\alpha} D(K^-) \mathcal{F}(\boldsymbol{p}_i^2), \tag{63}$$

where the vertex function $V_{1\mu}$ has been defined in Eq. (31) and $V_{2\alpha}$ has the following form:

$$V_{2\alpha} = -ie(\hat{Q}K^{*+}) R g_{VK^{*+}K^-} \epsilon_{\delta\beta\alpha\lambda} \epsilon_\gamma^\delta p_V^\beta \epsilon_V^\lambda. \tag{64}$$

It is obvious that the intermediate charge neutral loops cannot contribute since the amplitude is proportional to the charge of the pseudoscalar meson. Moreover, taking into account the SU(3) relation among the couplings, one finds that the two amplitudes with the intermediate $K^{*-}K^+$ and $K^{*+}K^-$ loops are constructive for all the decay channels into $\gamma\phi$, $\gamma\omega$, and $\gamma\rho^0$.

The detailed expressions of the loop amplitudes defined in this subsection are provided in the Appendix. Meanwhile, taking the advantage of the antisymmetric tensor structure for the VVP ($V\gamma P$) coupling, we can define effective couplings for each transition amplitude, and the total amplitude can be written as a sum of all these amplitudes, i.e.,

$$i\mathcal{M}_{\text{Total}} = i(g^T_{\eta_X\gamma V} + g^L_{\eta_X\gamma V}) \epsilon_{\alpha\beta\delta\lambda} p_\gamma^\alpha p_V^\beta \epsilon_\gamma^\delta \epsilon_V^\lambda, \tag{65}$$

where $g^T_{\eta_X\gamma V}$ and $g^L_{\eta_X\gamma V}$ are the effective couplings extracted from the tree and loop transitions, respectively.

III. NUMERICAL RESULTS AND DISCUSSIONS

The present experimental measurements of the exclusive decays of $\eta(1295)$ and $\eta(1405)$ are still far from satisfactory. In particular, the mass degeneracy of $f_1(1285)$ and $f_1(1420)$ with $\eta(1295)$ and $\eta(1405)$ has brought a lot of challenges to the data analysis. At this moment, the data from J/ψ and $\psi(3686)$ decays provide the joint branching ratios for the production and decay of these two states.

TABLE IX. Partial decay widths of $\eta_X \to \gamma V$ (in unit of MeV) calculated by the exclusive tree-level amplitudes, and two values $\Lambda = 0.75$ and 1.0 GeV for the cut-off energy are adopted as a comparison.

	Channels	Widths (tree amp.)	Widths (all) with $\Lambda =$ 0.75 GeV	Widths (all) with $\Lambda =$ 1.0 GeV
$\eta(1295)$	$\gamma\rho$	2.1 ± 0.6	2.5 ± 0.7	2.8 ± 0.7
	$\gamma\omega$	0.17 ± 0.06	0.26 ± 0.06	0.28 ± 0.06
	$\gamma\phi$	0.062 ± 0.02	0.19 ± 0.03	0.3 ± 0.03
$\eta(1405)$	$\gamma\rho$	2.7 ± 0.9	2.5 ± 0.8	2.5 ± 0.08
	$\gamma\omega$	0.23 ± 0.07	0.17 ± 0.06	0.14 ± 0.04
	$\gamma\phi$	0.19 ± 0.06	0.27 ± 0.07	0.33 ± 0.06

A. Partial decay widths for $\eta(1405)$ and $\eta(1295) \to \gamma V$

With the amplitudes and parameters provided in the previous section, we can directly calculate the radiative decays of these two states. In Table IX, the exclusive contributions from the tree-level amplitudes are listed and compared with the results with the loop contributions included. Two values for the cutoff parameter $\Lambda = 0.75$ and 1.0 GeV are adopted for the loop amplitudes to show the sensitivities of the partial decay widths to the loop contributions. It shows that the tree-level amplitude is dominant in $\eta(1405) \to \gamma\rho^0$, while relatively large loop interferences occur in $\eta(1405) \to \gamma\omega$ and $\gamma\phi$. Similar phenomena appear in the $\eta(1295)$ decays. One can see the dominance of the tree-level transition amplitude in $\eta(1295) \to \gamma\rho^0$, while the loop transitions have relatively large interference effects in $\eta(1295) \to \gamma\omega$ and $\gamma\phi$. In particular, the loop contributions in $\eta(1295) \to \gamma\phi$ turn out to be dominant. This is understandable since $\eta(1295)$ has large couplings to $K^*\bar{K} + \text{c.c.}$ in the mixing scheme, which will strongly enhance the loop amplitude. Moreover, the tree-level amplitude is suppressed by the intermediate $\phi \to e^+e^-$ coupling in the VMD model.

We can also examine the exclusive contributions from each loop diagram in order to clarify their roles in the interference with the tree-level amplitude. The results are listed in Table X for two cutoff values, i.e., $\Lambda = 0.75$ and 1.0 GeV. It shows that the triangle diagrams [Fig. 1(b)] have much smaller contributions than the contact diagrams [Figs. 1(c) and (d)]. Since both the $\gamma\omega$ and $\gamma\phi$ channels experience relatively large interferences from the loop transitions, it may lead to significant changes to the branching ratio fractions among these channels if compared with the tree-level results. It should also be noted that dependence of the interference effects on the cutoff parameter implies that a combined analysis of all the channels with constraints from experimental data is necessary. In the next subsection, we will show that the branching ratio fractions

TABLE X. Decay widths of each type of the hadronic loop diagrams with the cutoff parameter $\Lambda = 0.75$ and 1.0 GeV.

		$\Lambda = 0.75$ GeV		$\Lambda = 1.0$ GeV	
Diagrams	Decay channels (KeV)	$\eta(1295)$	$\eta(1405)$	$\eta(1295)$	$\eta(1405)$
$[K^*, \bar{K}, (K)]$	$\gamma\rho$	0.48	0.39	2.54	1.33
	$\gamma\omega$	0.038	0.034	0.21	0.16
	$\gamma\phi$	0.70	0.37	1.33	0.78
$[K^*, \bar{K}, (K^*)]$	$\gamma\rho$	5.73	2.63	10.0	7.63
	$\gamma\omega$	5.45	2.4	8.65	3.4
	$\gamma\phi$	4.56	2.83	5.3	3.25
$[K^*, \bar{K}^*, (K)]$	$\gamma\rho$	0.12	2.16	0.55	10.7
	$\gamma\omega$	6.8×10^{-3}	0.20	0.031	0.98
	$\gamma\phi$	8.2×10^{-3}	0.38	0.031	1.54
$[K^*, \bar{K}^*, (K^*)]$	$\gamma\rho$	0.044	1.46	0.15	5.1
	$\gamma\omega$	0.036	1.22	0.12	4.22
	$\gamma\phi$	0.051	2.68	0.15	7.97
$[K, \bar{K}^*, (K)]$	$\gamma\rho$	5.8×10^{-3}	3.8×10^{-3}	0.073	0.028
	$\gamma\omega$	4.9×10^{-3}	3.2×10^{-3}	0.06	0.024
	$\gamma\phi$	0.012	0.013	0.087	0.058
$[K, \bar{K}^*, (K^*)]$	$\gamma\rho$	6.1	1.16	29.3	3.35
	$\gamma\omega$	1.16	0.43	3.91	0.16
	$\gamma\phi$	0.8	0.69	3.9	3.39
$[K^*, \bar{K}]$	$\gamma\rho$	85.3	17	193.3	42.3
	$\gamma\omega$	82.3	16.6	185.4	41.1
	$\gamma\phi$	73.2	23.1	149.4	51.2
All loops	$\gamma\rho$	84.0	8.5	264.6	20.9
	$\gamma\omega$	43.9	11.7	111.6	43.8
	$\gamma\phi$	57.4	15.4	158.0	64.6

between different decay channels can provide further constraints on the role of the loop transitions.

B. Relative production rate between $\eta(1405)$ and $\eta(1295)$

To extract information about their internal structures, we define several branching ratio fractions which can be directly compared with the experimental data. For the production and decay of $\eta(1295)$ and $\eta(1405)$ in the same channel, we define

$$\mathcal{R}_\rho \equiv \frac{\Gamma_{J/\psi\to\gamma\eta(1405)\to\gamma\gamma\rho}}{\Gamma_{J/\psi\to\gamma\eta(1295)\to\gamma\gamma\rho}},$$
$$\mathcal{R}_\omega \equiv \frac{\Gamma_{J/\psi\to\gamma\eta(1405)\to\gamma\gamma\omega}}{\Gamma_{J/\psi\to\gamma\eta(1295)\to\gamma\gamma\omega}},$$
$$\mathcal{R}_\phi \equiv \frac{\Gamma_{J/\psi\to\gamma\eta(1405)\to\gamma\gamma\phi}}{\Gamma_{J/\psi\to\gamma\eta(1295)\to\gamma\gamma\phi}}. \tag{66}$$

With the amplitudes given in the previous section, we can first examine the branching ratio fractions contributed by the tree diagram in Fig. 1. As an example, the fraction $\mathcal{R}_\rho$ has the expression from the tree-level transitions

$$\mathcal{R}_\rho = \left(\frac{|\mathbf{p}_{\eta(1405)}|}{|\mathbf{p}_{\eta(1295)}|}\right)^3 \left(\frac{|\mathbf{p}_\rho|}{|\mathbf{p}'_\rho|}\right)^3 \left(\frac{m_L\Gamma_L}{m_H\Gamma_H}\right)^2 \times \left(\frac{\sqrt{2}\tan\alpha_P + R}{\sqrt{2} - R\tan\alpha_P}\right)^2 \tan^2\alpha_P, \tag{67}$$

where $\mathbf{p}_{\eta(1405)}$ and $\mathbf{p}_{\eta(1295)}$ denote the three-vector momenta of $\eta(1405)$ and $\eta(1295)$ in the J/ψ rest frame, respectively; $\mathbf{p}_\rho$ and $\mathbf{p}'_\rho$ are the final-state vector meson momenta in the rest frame of $\eta(1405)$ and $\eta(1295)$, respectively. This ratio is likely to be larger than unity given that $\alpha_P \simeq 42°$ in the scenario of the first radial excitations. Similarly, the ratios $\mathcal{R}_\omega$ and $\mathcal{R}_\phi$ from the tree diagrams can be extracted.

In Table XI, these three branching ratio fractions from the tree diagrams are listed. It shows that the combined branching ratio for $\eta(1405)$ is about 1 order of magnitude larger than that for $\eta(1295)$. This is consistent with the experimental observations that the signal for $\eta(1295)$ is significantly suppressed in the J/ψ radiative decays.

The inclusion of the loop processes introduces sizeable corrections to the branching ratio fractions, as we have learned earlier. In Table XI, the calculation results of $\mathcal{R}_\rho$, $\mathcal{R}_\omega$, and $\mathcal{R}_\phi$ with the loop contributions are also listed.

TABLE XI. Numerical results of $\mathcal{R}_\rho$, $\mathcal{R}_\omega$, and $\mathcal{R}_\phi$ with SU(3)-breaking factor $R = 0.8$, cutoff energy $\Lambda = 0.75$ GeV, and mixing angle $\alpha_P = 42°$. Here, we only list the values calculated with the central value of coupling g_{XVV}.

$\Lambda = 0.75$ GeV	$\mathcal{R}_\rho$	$\mathcal{R}_\omega$	$\mathcal{R}_\phi$
Tree level	10.8	10.9	20.8
T + L	8.8	6.0	12.5

The results marked with "Tree level" and "T + L" distinguish the situations of whether or not to include the loop contributions. Note again that Fig. 1(c) always vanishes. It shows that the inclusion of the loop diagrams has led to significant corrections to both $\mathcal{R}_\omega$ and $\mathcal{R}_\phi$. In contrast, $\mathcal{R}_\rho$ appears to be a relatively stable quantity. This is due to the dominance of the tree diagrams in $\gamma\rho^0$ for both $\eta(1405)$ and $\eta(1295)$.

C. Branching ratio fractions between different radiative decay channels

For $\eta(1295)$ or $\eta(1405)$ radiative decays into different channels, we define the following branching ratio fractions:

$$\begin{aligned}
\mathcal{R}^{\rho/\phi}_{\eta(1405)} &\equiv \frac{\Gamma_{\eta(1405)\to\gamma\rho}}{\Gamma_{\eta(1405)\to\gamma\phi}},\\
\mathcal{R}^{\phi/\omega}_{\eta(1405)} &\equiv \frac{\Gamma_{\eta(1405)\to\gamma\phi}}{\Gamma_{\eta(1405)\to\gamma\omega}},\\
\mathcal{R}^{\rho/\phi}_{\eta(1295)} &\equiv \frac{\Gamma_{\eta(1295)\to\gamma\rho}}{\Gamma_{\eta(1295)\to\gamma\phi}},\\
\mathcal{R}^{\omega/\phi}_{\eta(1295)} &\equiv \frac{\Gamma_{\eta(1295)\to\gamma\omega}}{\Gamma_{\eta(1295)\to\gamma\phi}}.
\end{aligned} \tag{68}$$

Note that the fractions in Eq. (68) are defined in such a way that the values at leading order will be larger than unity if $\eta(1295)$ and $\eta(1405)$ are the first radial excitations of η and η', respectively.

Supposing that only the tree-level amplitudes contribute in $\eta_X \to \gamma V$, the branching ratio fractions defined in Eq. (68) would have simple forms in terms of the mixing angle. As an example, the ratio between the $\gamma\rho^0$ and $\gamma\phi$ decay channel can be written as

$$\mathcal{R}^{\rho/\phi}_{\eta(1405)} \equiv \frac{\Gamma_{\eta(1405)\to\gamma\rho}}{\Gamma_{\eta(1405)\to\gamma\phi}} = \left(\frac{|\mathbf{p}_\rho|}{|\mathbf{p}_\phi|}\right)^3 \left[\frac{(em_\rho^2/f_\rho)G_\rho}{(em_\phi^2/f_\phi)G_\phi}\right]^2 \frac{\tan^2\alpha_P}{2R^2}, \tag{69}$$

where $\mathbf{p}_\rho$ and $\mathbf{p}_\phi$ are the three-vector momenta of the final-state ρ^0 and ϕ in the initial $\eta(1405)$ rest frame. By including the loop amplitudes, the branching ratio fractions will deviate from the above expectation.

As mentioned in the Introduction that the BESIII Collaboration recently measured the radiative decay of $\eta(1405) \to \gamma\phi$ in $J/\psi \to \gamma\gamma\phi$ [41], we can thus calculate $\mathcal{R}^{\rho/\phi}_{\eta(1405)}$ and compare it with the data. The results are presented in Fig. 2 in terms of two parameters α_P and $m_{\eta(1405)}$. These two variables are closely related to the interpretation of these two pseudoscalars. Therefore, the dependence of $\mathcal{R}^{\rho/\phi}_{\eta(1405)}$ on these two variables can illustrate whether it is a reasonable picture to treat these two states as the first radial excitation states

1. $\eta(1405) \to \gamma V$

In Fig. 2, the two overlapping bands denote the ranges of the experimental ratios extracted from the two solutions for $J/\psi \to \gamma\eta(1405/1475) \to \gamma\gamma\phi$ at BESIII [41] as listed in

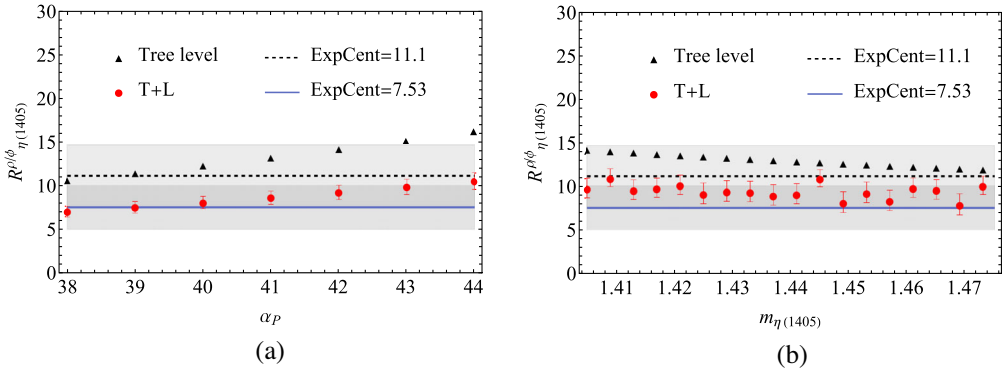

FIG. 2. (a) Dependence of $\mathcal{R}^{\rho/\phi}_{\eta(1405)}$ on the mixing angle α_P with $m_{\eta(1405)}$ fixed at 1.405 GeV. The solid dots and triangles denote the full calculation results and tree-level results, respectively. (b) Dependence of $\mathcal{R}^{\rho/\phi}_{\eta(1405)}$ on the mass of $\eta(1405)$ with the mixing angle α_P set at 42°. The solid dots and triangles have the same meaning as (a). In both figures, the cutoff energy $\Lambda = 0.75$ GeV is adopted; "T + L" denotes the full calculations including the tree and loop contributions. "ExpCent" denotes the central value of the two solutions from the BESIII analysis of $\mathcal{R}^{\rho/\phi}_{\eta(1405)}$, i.e., 11.10 ± 3.50 and 7.53 ± 2.49, respectively [41]. The light and dark gray bands indicate the error bars of the two solutions.

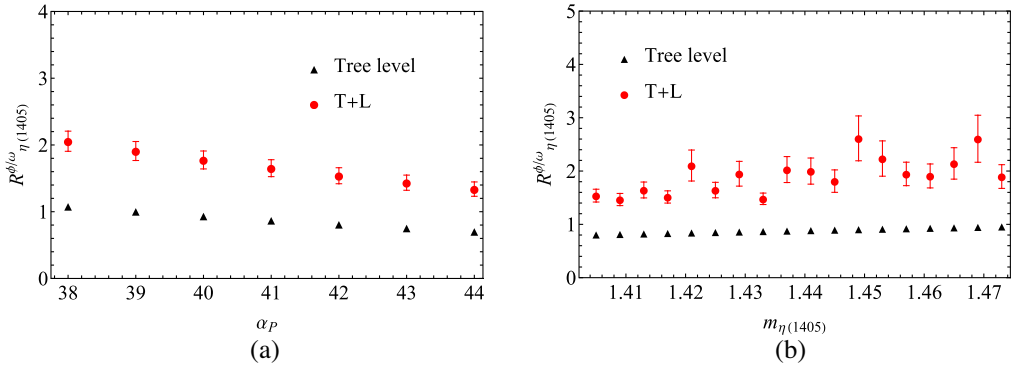

FIG. 3. (a) The dependence of $\mathcal{R}^{\phi/\omega}_{\eta(1405)}$ on the mixing angle α_P with $\Lambda = 0.75$ GeV and $m_{\eta(1405)} = 1.405$ GeV. (b) The dependence of $\mathcal{R}^{\phi/\omega}_{\eta(1405)}$ on the mass of $\eta(1405)$ with the mixing angle $\alpha_P = 42°$. In both figures, the cutoff energy $\Lambda = 0.75$ GeV is adopted. The legends of the symbols are the same as those in Fig. 2.

Table I. The central values, 7.53 ± 2.49 and 11.10 ± 3.50, are denoted by the solid and dashed lines, respectively. Within the commonly adopted values for α_P, i.e., $\alpha_P \simeq 38° \sim 44°$ [Fig. 2(a)] and within the mass region of $m_{\eta(1405)} = 1.405$~1.475 GeV [Fig. 2(b)], the ratios (round dots) are consistent with the data within the errors. Since we carry out numerical calculations of the loop integrals, we only present separated calculation results for demonstration. The errors with the round dots are given by the experimental errors with the data for $\eta(1405) \to \gamma\rho^0$ [45]. We also plot the ratios with only the tree amplitude (triangles) as a comparison. Again, the large discrepancies between the round dots and triangles indicate that the loop diagrams provide the significant interferences to the branching ratio fractions.

In Fig. 3, we present the predictions of $R^{\phi/\omega}_{\eta(1405)}$ for a range of α_P [Fig. 3(a)] and $m_{\eta(1405)}$ [Fig. 3(b)], similar to Fig. 2. The ratios turn out to be stable, and these two decays, i.e., $\eta(1405) \to \gamma\phi$ and $\gamma\omega$, are comparable to each other. Again, we see that the full amplitude calculations (round dots) are significantly different from the results with only the tree diagram contributions (triangles). This also indicates the dominant role played by the loop diagrams. The distributions of the round dots with errors show that the loop contributions are sensitive to the coupling of g_{XVV} determined by the data of $\eta(1405) \to \gamma\rho^0$.

Another aspect to be examined is the cutoff dependence of the branching ratio fractions. In Fig. 4, both ratios $R^{\rho/\phi}_{\eta(1405)}$ and $R^{\phi/\omega}_{\eta(1405)}$ in terms of a range of the cutoff parameter $\Lambda = 0.75$–1.0 GeV are presented in parts (a) and (b), respectively. It shows that $R^{\rho/\phi}_{\eta(1405)}$ is a stable quantity with the increasing Λ. Because of the dominance of the tree-level amplitude in $\eta(1405) \to \gamma\rho^0$, the errors with the round dots appear to be relatively smaller than those in $R^{\phi/\omega}_{\eta(1405)}$.

In Fig. 4(b), it shows that the ratio $R^{\phi/\omega}_{\eta(1405)}$ increases gradually in terms of Λ. This indicates the increasing contributions of the loop amplitudes in $\eta(1405) \to \gamma\phi$ with the increasing Λ. Combining Figs. 4(a) and 4(b) together, one can see that the relation $\Gamma_{\eta(1405)\to\gamma\rho^0} > \Gamma_{\eta(1405)\to\gamma\phi} > \Gamma_{\eta(1405)\to\gamma\omega}$, which is consistent with the expectation of the first radial excitation assignment

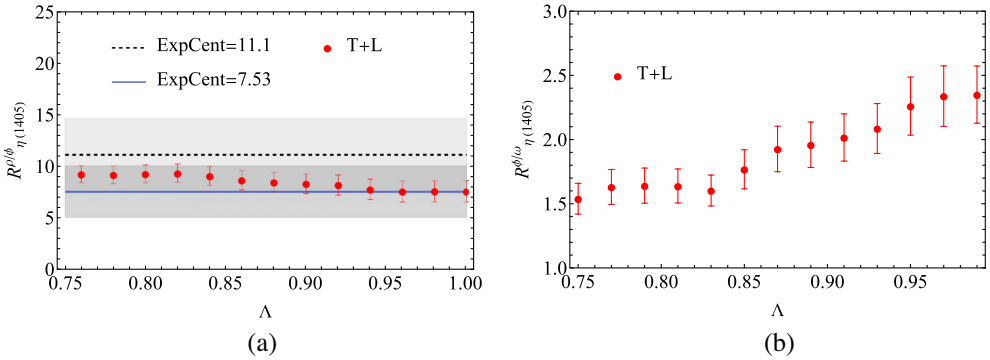

FIG. 4. The dependence of $\mathcal{R}^{\rho/\phi}_{\eta(1405)}$ [Fig. 4(a)] and $\mathcal{R}^{\phi/\omega}_{\eta(1405)}$ [Fig. 4(b)] on the cutoff energy Λ, with $\alpha_P = 42°$ and $m_{\eta(1405)} = 1.405$ GeV fixed in the calculations. The light and dark gray bands in (a) indicate the two solutions from the BESIII analysis, 7.53 ± 2.49 and 11.10 ± 3.50, respectively [41], and the central values are denoted by the solid and dashed lines, respectively.

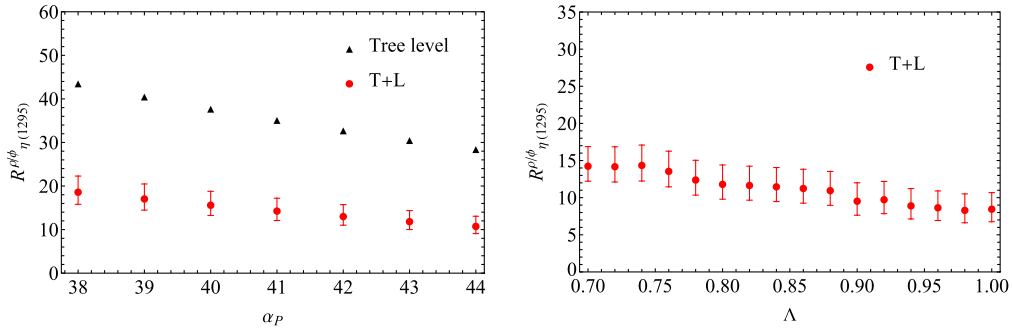

FIG. 5. (a) The dependence of $\mathcal{R}^{\rho/\phi}_{\eta(1295)}$ on the mixing angle α_P with $\Lambda = 0.75$ GeV. The tree-level results are denoted by the triangles, while the full calculation results are denoted by the solid round dots. (b) The dependence of $\mathcal{R}^{\rho/\phi}_{\eta(1295)}$ on the cutoff energy Λ with $\alpha_P = 42°$.

[29,34]. Also, the ratio $\mathcal{R}^{\rho/\phi}_{\eta(1405)}$ favors the solution of 7.53 ± 2.49 in Ref. [41].

2. $\eta(1295) \to \gamma V$

In Fig. 5(a), the predicted ratio $R^{\rho/\phi}_{\eta(1295)}$ in terms of the mixing angle α_P is plotted. The full calculation is denoted by the solid round dots, while the results for the exclusive tree-level transition are denoted by the triangles. Their difference indicates the significant interferences from the loop diagrams.

In Fig. 5(b), the dependence of $R^{\rho/\phi}_{\eta(1295)}$ on the cutoff parameter Λ is shown by the solid round dots. Within the range of $\Lambda = 0.75\sim1.0$ GeV, the ratio remains stable, although a decreasing tendency appears with the increasing Λ.

In Fig. 6, the ratio $R^{\omega/\phi}_{\eta(1295)}$ is calculated and presented in a similar way as in Fig. 5. We can see that the dependence of the ratios on the mixing angle α_P [Fig. 6(a)] is similar to $R^{\rho/\phi}_{\eta(1295)}$. We also investigate the cutoff dependence of the loop transition contributions, and the results are presented in Fig. 6(b). Again, we find that the ratio keeps stable.

The present calculation results favor that $R^{\rho/\phi}_{\eta(1405)}$ takes the lower ratio 7.53 ± 2.49 in Ref. [41], and its dependence of the form factor parameter appears to be stable. However, we should caution that the experimental ratio strongly depends on the data for $\eta(1405) \to \gamma\rho^0$ [40], which still contain large errors. Meanwhile, the two experimental solutions are for the constructive and destructive interferences from $X(1835)$ in Ref. [41], which means a combined partial wave analysis is required for more quantitative studies. Such uncertainties will affect our determination of the parameter g_{XVV} and influence the loop interfering patterns.

D. Loop influence on the mixing angle

The above studies have shown the impact of the loop transitions on the experimental observables defined in the productions and decays of $\eta(1295)$ and $\eta(1405)$ in $J/\psi \to \gamma\gamma V$. As a consequence, it implies that the measured mixing angle between $\eta(1295)$ and $\eta(1405)$ may possess different values in different processes if the detailed transition mechanisms have not been properly included.

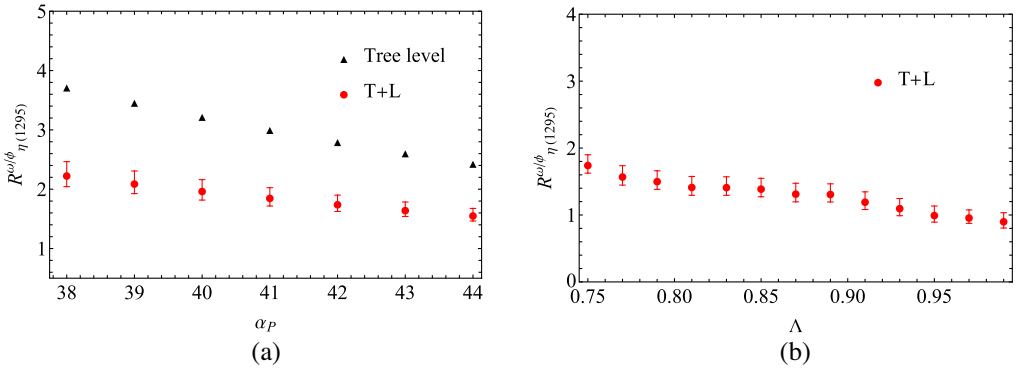

FIG. 6. (a) The dependence of $R^{\omega/\phi}_{\eta(1295)}$ on the mixing angle α_P with $\Lambda = 0.75$ GeV. (b) The dependence of $R^{\omega/\phi}_{\eta(1295)}$ on parameter Λ with the mixing angle $\alpha_P = 42°$. The legends are the same as Fig. 5.

To illustrate this, we adopt Eq. (69) as an example. Without the loop transitions, Eq. (69) will define a mixing angle which can be extracted with the experimental value of $\mathcal{R}^{\rho/\phi}_{\eta(1405)}$ as the input. But if the loop transitions are included, the ratio should be expressed as

$$\mathcal{R}^{\rho/\phi}_{\eta(1405)} \equiv \frac{\Gamma_{\eta(1405)\to\gamma\rho}}{\Gamma_{\eta(1405)\to\gamma\phi}} = \left(\frac{|\mathbf{p}_\rho|}{|\mathbf{p}_\phi|}\right)^3 \left[\frac{g^T_{\eta(1405)\gamma\rho}(\alpha_P)+g^L_{\eta(1405)\gamma\rho}(\alpha_P)}{g^T_{\eta(1405)\gamma\phi}(\alpha_P)+g^L_{\eta(1405)\gamma\phi}(\alpha_P)}\right]^2. \tag{70}$$

By matching it to the tree-level relation defined in Eq. (69), one has

$$\left[\frac{(em^2_\rho/f_\rho)G_\rho}{(em^2_\phi/f_\phi)G_\phi}\right]^2 \frac{\tan^2\tilde{\alpha}_P}{2R^2} \equiv \left[\frac{g^T_{\eta(1405)\gamma\rho}(\alpha_P)+g^L_{\eta(1405)\gamma\rho}(\alpha_P)}{g^T_{\eta(1405)\gamma\phi}(\alpha_P)+g^L_{\eta(1405)\gamma\phi}(\alpha_P)}\right]^2, \tag{71}$$

and the "empirical" mixing angle $\tilde{\alpha}_P$ can be extracted. In Table XII, we list the extracted values of $\tilde{\alpha}_P$ from the ratios $R^{\rho/\phi}_{\eta(1405)}$ and $R^{\rho/\phi}_{\eta(1295)}$. With three values for α_P in the calculations as an illustration, we see that the extracted values for the mixing angle $\tilde{\alpha}_P$ are different in the measurements of these two ratios. To some extent, the deviations of $\tilde{\alpha}_P$ from the commonly adopted values could be acceptable in a single channel. However, when putting two channels together, such deviations should be regarded as significant. Further experimental measurements of these ratios would be able to clarify the role played by the loop transitions.

IV. SUMMARY

In this work, based on the one-state assumption for $\eta(1405)$ and $\eta(1475)$, we systematically investigate the radiative decays of $\eta(1295)$ and $\eta(1405)$ by treating them as the first radial excitations of η and η'. In the framework of the VMD model, we include the intermediate $\bar{K}K^* + \text{c.c.}$ meson loops as the leading correction to the tree-level transition amplitudes for the $\eta(1295)$ and $\eta(1405) \to \gamma V$. With an exponential form factor for the regularization of the loop integrals, we are able to to understand the production and decay behavior of both states in the J/ψ radiative decays. In particular, the radiative decays of $\eta(1405) \to \gamma V$ can be described in agreement with the BESIII measurement. It is interesting to note that the loop transitions can produce significant effects in some decay channels. For instance, the loop contributions in $\eta(1295) \to \gamma\phi$ are found to be compatible with the tree-level contributions. This should not be surprising since the coupling of $g_{\eta(1295)K^*K}$ in the loop amplitude is sizeable and the ϕ meson decay constant in the tree-level amplitude is much smaller than that of the ρ^0 meson (see Table II). Since the production of $\eta(1295)$ in $J/\psi \to \gamma\gamma\rho^0$ has the largest branching ratio, experimental study of $\eta(1295)$ in this channel is strongly recommended for testing the relations presented in this work.

TABLE XII. Extracting a new mixing angle $\tilde{\alpha}_P$ for the given mixing angle α_P with cut off parameter $\Lambda = 0.75$ GeV.

	$\tilde{\alpha}_P$	
α_P	$R^{\rho/\phi}_{\eta(1295)}$	$R^{\rho/\phi}_{\eta(1405)}$
42°	54.9°	32.4°
40°	52.4°	34.2°
38°	50°	36°

In the scenario of assigning $\eta(1295)$ and $\eta(1405)$ as the first radial excitation states of η and η', we show that the branching ratio fractions between these two states in the same decay channel, or between two exclusive decay channels for the same state, exhibit interesting patterns when the intermediate $\bar{K}K^* + \text{c.c.}$ meson loops are properly included. Due to the loop corrections, the mixing angle extracted from the radiative decay data will be affected by the loop correction effects. It would be different from the commonly adopted one extracted in other processes. We also find that the contributions from the meson loops are relatively small in $\eta(1405)$ and $\eta(1295) \to \gamma\rho^0$. Thus, this channel will be dominated by the tree-level transition and is ideal for extracting the mixing angle.

In brief, we find that the radiative decays of $J/\psi \to \gamma\gamma V$ can serve as a probe for understanding the nature of $\eta(1295)$ and $\eta(1405)$. With the large data sample of J/ψ at BESIII, we can disentangle the role played by the meson loop transitions and gain more insights into the pseudoscalar meson spectrum.

ACKNOWLEDGMENTS

This work is supported, in part, by the National Natural Science Foundation of China (Grants No. 11425525 and No. 11521505), DFG and NSFC funds to the Sino-German CRC 110 "Symmetries and the Emergence of Structure in QCD" (NSFC Grant No. 12070131001 and DFG Project No. 196253076), National Key Basic Research Program of China under Contract No. 2020YFA0406300, and Strategic Priority Research Program of Chinese Academy of Sciences (Grant No. XDB34030302).

APPENDIX A: AMPLITUDES OF THE HADRONIC LOOP DIAGRAMS

In this Appendix, we present the loop amplitudes for the convenience of tracking the calculation details (for simplicity, we do not distinguish the coupling constants at the hadronic vertices but just denote them as g_i with $i = 1, 2, 3$):

(i) $[K^*, \bar{K}, (K)]$:

$$\begin{aligned}
i\mathcal{M} &= g_1 g_2 g_3 \int \frac{d^4 p_1}{(2\pi)^4} (p_X + p_3)_\sigma \frac{(g^{\sigma\mu} - \frac{p_1^\sigma p_1^\mu}{p_1^2})}{p_1^2 - m_{K^*}^2 + i\epsilon} \epsilon_{\alpha\beta\delta\mu} p_\gamma^\alpha p_1^\beta \epsilon_\gamma^\delta \frac{(p_2 - p_3)_\lambda \epsilon_V^\lambda}{(p_2^2 - m_K^2 + i\epsilon)(p_3^2 - m_K^2 + i\epsilon)} \mathcal{F}(\boldsymbol{p}_i^2) \\
&= g_1 g_2 g_3 \int \frac{d^4 p_1}{(2\pi)^4} \frac{\epsilon_{\alpha\beta\delta\mu} p_\gamma^\alpha p_1^\beta \epsilon_\gamma^\delta (2p_\gamma + 2p_V - p_1)^\mu (2p_1 - 2p_\gamma - p_V)_\lambda \epsilon_V^\lambda}{(p_1^2 - m_{K^*}^2 + i\epsilon)(p_2^2 - m_K^2 + i\epsilon)(p_3^2 - m_K^2 + i\epsilon)} \mathcal{F}(\boldsymbol{p}_i^2) \\
&= 2 g_1 g_2 g_3 \epsilon_{\alpha\beta\delta\mu} p_\gamma^\alpha p_V^\mu \epsilon_\gamma^\delta \epsilon_V^\lambda \int \frac{d^4 p_1}{(2\pi)^4} \frac{p_1^\beta [2(p_1)_\lambda - (2p_\gamma + p_V)_\lambda]}{(p_1^2 - m_{K^*}^2 + i\epsilon)(p_3^2 - m_K^2 + i\epsilon)(p_2^2 - m_K^2 + i\epsilon)} \mathcal{F}(\boldsymbol{p}_i^2) \\
&= 2 g_1 g_2 g_3 \epsilon_{\alpha\beta\delta\mu} p_\gamma^\alpha p_V^\mu \epsilon_\gamma^\delta \epsilon_V^\lambda \int \frac{d^4 p_1}{(2\pi)^4} \frac{2 p_1^\beta p_{1\lambda}}{(p_1^2 - m_{K^*}^2 + i\epsilon)(p_3^2 - m_K^2 + i\epsilon)(p_2^2 - m_K^2 + i\epsilon)} \mathcal{F}(\boldsymbol{p}_i^2). \qquad \text{(A1)}
\end{aligned}$$

Note that, due to the property of the antisymmetric tensor, only the δ_λ^β term could survive in the tensor integral.

(ii) $[K^*, \bar{K}, (K^*)]$:

$$\begin{aligned}
i\mathcal{M} = & \int \frac{d^4 p_1}{(2\pi)^4} \frac{g_1 g_2 g_3 (p_X + p_3)_\sigma (g^{\sigma\mu} - \frac{p_1^\sigma p_1^\mu}{p_1^2})(g^{\rho\nu} - \frac{p_2^\rho p_2^\nu}{p_2^2}) \epsilon_{\alpha\beta\nu\lambda} p_2^\alpha p_V^\beta \epsilon_V^\lambda}{(p_1^2 - m_{K^*}^2)(p_2^2 - m_{K^*}^2)(p_3^2 - m_K^2)} \\
& \times [\epsilon_\gamma^\delta g_{\delta\mu} p_{1\rho} + \epsilon_\gamma^\delta g_{\delta\rho} p_{2\mu} - g_{\mu\rho} (p_1 + p_2)_\delta \epsilon_\gamma^\delta] \mathcal{F}(\boldsymbol{p}_i^2) \\
= & \, g_1 g_2 g_3 \int \frac{d^4 p_1}{(2\pi)^4} \frac{-2}{p_1^2 (p_1^2 - m_{K^*}^2)(p_2^2 - m_{K^*}^2)(p_3^2 - m_K^2)} \\
& \times \{\epsilon_{\alpha\beta\nu\lambda} p_\gamma^\alpha p_V^\beta \epsilon_\gamma^\nu \epsilon_V^\lambda [(p_1 \cdot p_\gamma)^2 - p_1^2 (p_V \cdot p_\gamma) + (p_1 \cdot p_\gamma)(p_1 \cdot p_V)] \\
& - \epsilon_{\alpha\beta\nu\lambda} p_1^\alpha p_V^\beta \epsilon_\gamma^\nu \epsilon_V^\lambda [(p_1 \cdot p_\gamma)^2 - p_1^2 (p_V \cdot p_\gamma) + (p_1 \cdot p_\gamma)(p_1 \cdot p_V)] \\
& - \epsilon_{\alpha\beta\nu\lambda} p_\gamma^\alpha p_V^\beta p_1^\nu \epsilon_V^\lambda [(p_1 \cdot \epsilon_\gamma - p_\gamma \cdot \epsilon_\gamma)(2p_1^2 - p_1 \cdot p_\gamma - p_1 \cdot p_V) - p_1^2 (p_V \cdot \epsilon_\gamma)]\} \mathcal{F}(\boldsymbol{p}_i^2). \qquad \text{(A2)}
\end{aligned}$$

In the above integral, after contracting the Lorentz indices, the amplitude can be simplified to a more compact form. One notices that the first term in the big brackets is a scalar integral, while the second and third terms will pick up the linear terms containing p_γ^α and ϵ_γ^ν, respectively, due to the property of the antisymmetric tensor. The same analysis is also applied to the following loop amplitudes.

(iii) $[K^*, \bar{K}^*, (K)]$:

$$\begin{aligned}
i\mathcal{M} = & \, g_1 g_2 g_3 \int \frac{d^4 p_1}{(2\pi)^4} \frac{\epsilon_{\alpha\beta\mu\nu} p_1^\alpha p_3^\beta (g^{\mu\mu'} - \frac{p_1^\mu p_1^{\mu'}}{p_1^2}) \epsilon_{\alpha_1\beta_1\mu'\delta} p_1^{\alpha_1} p_\gamma^{\beta_1} \epsilon_\gamma^\delta \epsilon_{\alpha_2\beta_2\nu'\lambda} p_3^{\alpha_2} p_V^{\beta_2} \epsilon_V^\lambda (g^{\nu\nu'} - \frac{p_3^\nu p_3^{\nu'}}{p_3^2})}{(p_1^2 - m_{K^*}^2)(p_2^2 - m_K^2)(p_3^2 - m_{K^*}^2)} \mathcal{F}(\boldsymbol{p}_i^2) \\
= & \, g_1 g_2 g_3 \int \frac{d^4 p_1}{(2\pi)^4} \frac{\epsilon_{\alpha\beta\mu\nu} p_1^\alpha p_3^\beta \times \epsilon_{\alpha_1\beta_1\mu\delta} p_1^{\alpha_1} p_\gamma^{\beta_1} \epsilon_\gamma^\delta \times \epsilon_{\alpha_2\beta_2\nu\lambda} p_3^{\alpha_2} p_V^{\beta_2} \epsilon_V^\lambda}{(p_1^2 - m_{K^*}^2)(p_2^2 - m_K^2)(p_3^2 - m_{K^*}^2)} \mathcal{F}(\boldsymbol{p}_i^2) \\
= & \, g_1 g_2 g_3 \int \frac{d^4 p_1}{(2\pi)^4} \frac{\mathcal{F}(\boldsymbol{p}_i^2)}{(p_1^2 - m_{K^*}^2)(p_2^2 - m_K^2)(p_3^2 - m_{K^*}^2)} \times \{\epsilon_{\alpha\beta\delta\lambda} p_\gamma^\alpha p_V^\beta \epsilon_\gamma^\delta \epsilon_V^\lambda [(p_1 \cdot p_\gamma)^2 + (p_1 \cdot p_\gamma)(p_1 \cdot p_V) - p_1^2 (p_V \cdot p_\gamma)] \\
& + \epsilon_{\alpha\beta\delta\lambda} p_1^\alpha p_V^\beta \epsilon_\gamma^\delta \epsilon_V^\lambda [-(p_1 \cdot p_\gamma)^2] + \epsilon_{\alpha\beta\delta\lambda} p_\gamma^\alpha p_1^\beta \epsilon_\gamma^\delta \epsilon_V^\lambda [(p_1 \cdot p_V)^2 - p_1^2 p_V^2] - \epsilon_{\alpha\beta\delta\lambda} p_\gamma^\alpha p_V^\beta p_1^\delta \epsilon_V^\lambda [(p_1 \cdot p_\gamma)(p_1 \cdot \epsilon_\gamma) \\
& - (p_V \cdot p_\gamma)(p_1 \cdot \epsilon_\gamma) + (p_1 \cdot p_\gamma)(p_V \cdot \epsilon_\gamma)] + \epsilon_{\alpha\beta\delta\lambda} p_\gamma^\alpha p_V^\beta \epsilon_\gamma^\delta p_1^\lambda [(p_1 \cdot p_V)(p_1 \cdot \epsilon_V)]\}. \qquad \text{(A3)}
\end{aligned}$$

(iv) $[K^*, \bar{K}^*, (K^*)]$:

$$
\begin{aligned}
i\mathcal{M} &= g_1 g_2 g_3 \int \frac{d^4 p_1}{(2\pi)^4} \frac{\epsilon_{\alpha\beta\mu\nu} p_1^\alpha p_3^\beta (g^{\mu\mu'} - \frac{p_1^\mu p_1^{\mu'}}{p_1^2})(g^{\rho\sigma} - \frac{p_2^\rho p_2^\sigma}{p_2^2})(g^{\nu\nu'} - \frac{p_3^\nu p_3^{\nu'}}{p_3^2})}{(p_1^2 - m_{K^*}^2)(p_2^2 - m_{K^*}^2)(p_3^2 - m_{K^*}^2)} \\
&\quad \times [\epsilon_\gamma^\delta g_{\delta\mu'} p_{1\rho} + \epsilon_\gamma^\delta g_{\delta\rho} p_{2\mu'} - g_{\mu'\rho}(p_1 + p_2)_\delta \epsilon_\gamma^\delta] \times [\epsilon_V^\lambda g_{\lambda\nu'} p_{3\sigma} - \epsilon_V^\lambda g_{\lambda\sigma} p_{2\nu'} + g_{\nu'\sigma}(p_2 - p_3)_\lambda \epsilon_V^\lambda] \mathcal{F}(\boldsymbol{p}_i^2), \\
&= g_1 g_2 g_3 \int \frac{d^4 p_1}{(2\pi)^4} \frac{\epsilon_{\alpha\beta\mu\nu} p_1^\alpha p_3^\beta (g^{\rho\sigma} - \frac{p_2^\rho p_2^\sigma}{p_2^2})}{(p_1^2 - m_{K^*}^2)(p_2^2 - m_{K^*}^2)(p_3^2 - m_{K^*}^2)} \\
&\quad \times [\epsilon_\gamma^\delta g_{\delta\mu} p_{1\rho} + \epsilon_\gamma^\delta g_{\delta\rho} p_{2\mu} - g_{\mu\rho}(p_1 + p_2)_\delta \epsilon_\gamma^\delta] \times [\epsilon_V^\lambda g_{\lambda\nu} p_{3\sigma} - \epsilon_V^\lambda g_{\lambda\sigma} p_{2\nu} + g_{\nu\sigma}(p_2 - p_3)_\lambda \epsilon_V^\lambda] \mathcal{F}(\boldsymbol{p}_i^2), \\
&= g_1 g_2 g_3 \int \frac{d^4 p_1}{(2\pi)^4} \frac{\mathcal{F}(\boldsymbol{p}_i^2)}{p_2^2 (p_1^2 - m_{K^*}^2)(p_2^2 - m_{K^*}^2)(p_3^2 - m_{K^*}^2)} \\
&\quad \times \{-\epsilon_{\alpha\beta\delta\lambda} p_1^\alpha p_V^\beta \epsilon_\gamma^\delta \epsilon_V^\lambda [p_2^2(-p_1 \cdot p_\gamma - p_1 \cdot p_V + p_1^2) + (p_1 \cdot p_\gamma - p_1^2)(-2(p_1 \cdot p_\gamma) + p_V \cdot p_\gamma - p_1 \cdot p_V + p_1^2)] \\
&\quad + \epsilon_{\alpha\beta\delta\lambda} p_\gamma^\alpha p_1^\beta \epsilon_\gamma^\delta \epsilon_V^\lambda [p_2^2(-p_1 \cdot p_\gamma - p_1 \cdot p_V + p_1^2) + (p_1 \cdot p_\gamma - p_1^2)(-2(p_1 \cdot p_\gamma) + p_V \cdot p_\gamma - p_1 \cdot p_V + p_1^2)] \\
&\quad - \epsilon_{\alpha\beta\delta\lambda} p_\gamma^\alpha p_V^\beta p_1^\delta \epsilon_V^\lambda [2p_2^2(p_1 \cdot \epsilon_\gamma) + p_2^2(p_1 \cdot \epsilon_\gamma - p_V \cdot \epsilon_\gamma) + (p_1 \cdot \epsilon_\gamma)(-2(p_1 \cdot p_\gamma) + p_V \cdot p_\gamma - p_1 \cdot p_V + p_1^2)] \\
&\quad + \epsilon_{\alpha\beta\delta\lambda} p_\gamma^\alpha p_V^\beta \epsilon_\gamma^\delta p_1^\lambda [2p_2^2(p_\gamma \cdot \epsilon_V) - 3p_2^2(p_1 \cdot \epsilon_V) - 2(p_1^2 - p_1 \cdot p_\gamma)(p_1 \cdot \epsilon_V) \\
&\quad + (p_1^2 - p_1 \cdot p_\gamma)(p_1 \cdot \epsilon_V - p_\gamma \cdot \epsilon_V) + 2(p_1^2 - p_1 \cdot p_\gamma)(p_\gamma \cdot \epsilon_V)]\}. \qquad \text{(A4)}
\end{aligned}
$$

(v) $[K, \bar{K}^*, (K)]$:

$$
\begin{aligned}
i\mathcal{M} &= \int \frac{d^4 p_1}{(2\pi)^4} g_1 g_2 g_3 \frac{(p_X + p_1)_\mu (p_1 + p_2)_\delta \epsilon_\gamma^\delta \epsilon_{\alpha\beta\nu\lambda} p_3^\alpha p_V^\beta \epsilon_V^\lambda (g^{\mu\nu} - \frac{p_3^\mu p_3^\nu}{p_3^2})}{(p_1^2 - m_K^2)(p_2^2 - m_K^2)(p_3^2 - m_{K^*}^2)} \mathcal{F}(\boldsymbol{p}_i^2) \\
&= g_1 g_2 g_3 \int \frac{d^4 p_1}{(2\pi)^4} \frac{\epsilon_{\alpha\beta\mu\lambda} p_3^\alpha p_V^\beta \epsilon_V^\lambda (2p_1 + p_3)^\mu (2p_1 - p_\gamma)_\delta \epsilon_\gamma^\delta}{(p_1^2 - m_K^2)(p_2^2 - m_K^2)(p_3^2 - m_{K^*}^2)} \mathcal{F}(\boldsymbol{p}_i^2) \\
&= g_1 g_2 g_3 \int \frac{d^4 p_1}{(2\pi)^4} \frac{\epsilon_{\alpha\beta\mu\lambda} p_3^\alpha p_V^\beta \epsilon_V^\lambda (2p_1)^\mu (2p_1)_\delta \epsilon_\gamma^\delta}{(p_1^2 - m_K^2)(p_2^2 - m_K^2)(p_3^2 - m_{K^*}^2)} \mathcal{F}(\boldsymbol{p}_i^2) \\
&= g_1 g_2 g_3 \int \frac{d^4 p_1}{(2\pi)^4} \frac{\epsilon_{\alpha\beta\mu\lambda} (p_\gamma + p_V - p_1)^\alpha p_V^\beta \epsilon_V^\lambda (2p_1)^\mu (2p_1)_\delta \epsilon_\gamma^\delta}{(p_1^2 - m_K^2)(p_2^2 - m_K^2)(p_3^2 - m_{K^*}^2)} \mathcal{F}(\boldsymbol{p}_i^2) \\
&= 4 g_1 g_2 g_3 \epsilon_{\alpha\beta\mu\lambda} p_V^\beta \epsilon_V^\lambda \epsilon_\gamma^\delta \int \frac{d^4 p_1}{(2\pi)^4} \frac{p_\gamma^\alpha p_1^\mu p_{1\delta} - p_1^\alpha p_1^\mu p_1^\delta}{(p_1^2 - m_K^2)(p_2^2 - m_K^2)(p_3^2 - m_{K^*}^2)} \mathcal{F}(\boldsymbol{p}_i^2) \\
&= 4 g_1 g_2 g_3 \epsilon_{\alpha\beta\mu\lambda} p_\gamma^\alpha p_V^\beta \epsilon_V^\lambda \epsilon_\gamma^\delta \int \frac{d^4 p_1}{(2\pi)^4} \frac{p_1^\mu p_{1\delta}}{(p_1^2 - m_K^2)(p_2^2 - m_K^2)(p_3^2 - m_{K^*}^2)} \mathcal{F}(\boldsymbol{p}_i^2). \qquad \text{(A5)}
\end{aligned}
$$

(vi) $[K, \bar{K}^*, (K^*)]$:

$$
\begin{aligned}
i\mathcal{M} &= g_1 g_2 g_3 \int \frac{d^4 p_1}{(2\pi)^4} \frac{(p_X + p_1)_\mu \epsilon_{\alpha\beta\nu\delta} p_2^\alpha p_\gamma^\beta \epsilon_\gamma^\delta (g^{\nu\nu'} - \frac{p_2^\nu p_2^{\nu'}}{p_2^2})(g^{\mu'\mu} - \frac{p_3^{\mu'} p_3^\mu}{p_3^2})}{(p_1^2 - m_K^2)(p_2^2 - m_{K^*}^2)(p_3^2 - m_{K^*}^2)} [\epsilon_V^\lambda g_{\lambda\mu'} p_{3\nu'} - \epsilon_V^\lambda g_{\lambda\nu'} p_{2\mu'} + g_{\mu'\nu'}(p_2 - p_3)_\lambda \epsilon_V^\lambda] \mathcal{F}(\boldsymbol{p}_i^2), \\
&= g_1 g_2 g_3 \int \frac{d^4 p_1}{(2\pi)^4} \frac{(p_X + p_1)_\mu \epsilon_{\alpha\beta\nu\delta} p_2^\alpha p_\gamma^\beta \epsilon_\gamma^\delta (g^{\mu'\mu} - \frac{p_3^{\mu'} p_3^\mu}{p_3^2})}{(p_1^2 - m_K^2)(p_2^2 - m_{K^*}^2)(p_3^2 - m_{K^*}^2)} \times [\epsilon_V^\lambda g_{\lambda\mu'} p_{3\nu} - \epsilon_V^\lambda g_{\lambda\nu} p_{2\mu'} + g_{\mu'\nu}(p_2 - p_3)_\lambda \epsilon_V^\lambda] \mathcal{F}(\boldsymbol{p}_i^2), \\
&= g_1 g_2 g_3 \int \frac{d^4 p_1}{(2\pi)^4} \frac{\mathcal{F}(\boldsymbol{p}_i^2)}{p_3^2 (p_1^2 - m_K^2)(p_2^2 - m_{K^*}^2)(p_3^2 - m_{K^*}^2)}
\end{aligned}
$$

$$\times\{-\epsilon_{\alpha\beta\delta\lambda}p_\gamma^\alpha p_1^\beta\epsilon_\gamma^\delta\epsilon_V^\lambda[2(p_\gamma\cdot p_V)^2+2p_1^2(p_1\cdot p_\gamma)-p_3^2(p_\gamma\cdot p_V)+p_3^2(p_1\cdot p_V)+p_3^2p_1^2+p_1^2(p_\gamma\cdot p_V)-2p_V^2(p_1\cdot p_\gamma)$$
$$-2(p_1\cdot p_V)(p_\gamma\cdot p_V)-4(p_1\cdot p_\gamma)(p_\gamma\cdot p_V)+p_V^2(p_\gamma\cdot p_V)+p_1^2p_V^2+p_1^2(p_1\cdot p_V)-p_V^2(p_1\cdot p_V)-p_1^4]$$
$$-\epsilon_{\alpha\beta\delta\lambda}p_\gamma^\alpha p_V^\beta\epsilon_\gamma^\delta p_1^\lambda[-p_3^2(p_\gamma\cdot\epsilon_V)+3p_3^2(p_1\cdot\epsilon_V)-p_1^2(p_\gamma\cdot\epsilon_V)-2(p_\gamma\cdot p_V)(p_1\cdot\epsilon_V)+p_V^2(p_\gamma\cdot\epsilon_V)$$
$$+2(p_\gamma\cdot p_V)(p_\gamma\cdot\epsilon_V)+p_1^2(p_1\cdot\epsilon_V)-p_V^2(p_1\cdot\epsilon_V)]\}. \tag{A6}$$

(vii) $[K^*,\bar{K}]$:

$$\begin{aligned}i\mathcal{M}&=eg_{\eta_X K^{*+}K^-}g_{VK^{*+}K^-}\int\frac{d^4p_1}{(2\pi)^4}\frac{(p_X+p_2)_\mu(g^{\mu\alpha}-\frac{p_1^\mu p_1^\alpha}{p_1^2})\epsilon_{\delta\beta\alpha\lambda}\epsilon_\gamma^\delta p_V^\beta\epsilon_V^\lambda}{(p_1^2-m_{K^*}^2)(p_2^2-m_K^2)}\mathcal{F}(\boldsymbol{p}_i^2).\\&=eg_1g_2\int\frac{d^4p_1}{(2\pi)^4}\frac{\epsilon_{\delta\beta\alpha\lambda}\epsilon_\gamma^\delta p_V^\beta\epsilon_V^\lambda(p_X+p_2)_\mu(g^{\mu\alpha}-\frac{p_1^\mu p_1^\alpha}{p_1^2})}{(p_1^2-m_{K^*}^2)(p_2^2-m_K^2)}\mathcal{F}(\boldsymbol{p}_i^2).\\&=eg_1g_2\int\frac{d^4p_1}{(2\pi)^4}\left\{\epsilon_{\alpha\beta\delta\lambda}p_1^\alpha p_V^\beta\epsilon_\gamma^\delta\epsilon_V^\lambda\frac{2(p_1\cdot p_\gamma+p_1\cdot p_V)}{p_1^2(p_1^2-m_{K^*}^2)(p_2^2-m_K^2)}-\frac{2\epsilon_{\alpha\beta\delta\lambda}p_\gamma^\alpha p_V^\beta\epsilon_\gamma^\delta\epsilon_V^\lambda}{(p_1^2-m_{K^*}^2)(p_2^2-m_K^2)}\right\}\mathcal{F}(\boldsymbol{p}_i^2).\end{aligned} \tag{A7}$$

APPENDIX B: COUPLING RELATION EXTRACTED IN THE $^3P_0$ MODEL

The VPP, VVP, and VVV couplings have dynamic connections in the quark model. Here, V and P are the ground-state vector and pseudoscalar $q\bar{q}$ mesons. Taking the ϕ meson couplings to $K\bar{K}$, $K^*\bar{K}$, and $K^*\bar{K}^*$ as an example, we can see that the spatial wave function overlaps only involve the ground states V and P and they can be treated the same at the leading order. Then, the coupling differences will arise from the spin-flavor structure in the transition operators. Note that the color factor is a trivial one and it is the same for all these couplings.

Considering the effective couplings at the hadronic level, we can write down the transition amplitudes as follows:

$$i\mathcal{M}_{VPP}=-ig_{\phi K^+K^-}(p_B-p_C)_\mu\epsilon_A^\mu, \tag{B1}$$

$$i\mathcal{M}_{VVP}=ig_{\phi K^*\bar{K}}\epsilon_{\alpha\beta\mu\nu}p_A^\alpha p_B^\beta\epsilon_A^\mu\epsilon_B^{\nu*}, \tag{B2}$$

$$i\mathcal{M}_{VVV}=-ig_{\phi K^*\bar{K}^*}[\epsilon_B^*\cdot\epsilon_C^*(p_B-p_C)\cdot\epsilon_A-\epsilon_B^*\cdot\epsilon_A(p_B\cdot\epsilon_C^*)+\epsilon_C^*\cdot\epsilon_A(p_C\cdot\epsilon_B^*)]. \tag{B3}$$

The same processes can also be described by the quark model formalism, and we adopt the quark pair creation model (i.e., $^3P_0$ model) [49] to extract the coupling in the quark model.

For an Okubo-Zweig-Iizuka (OZI)-allowed decay of $A\to BC$, the general form of the transition matrix element is [50]

$$\begin{aligned}\mathcal{M}^{M_{J_A}M_{J_B}M_{J_C}}(\vec{P})&=\gamma\sqrt{8E_AE_BE_C}\sum_{\substack{M_{L_A},M_{S_A},M_{L_B},M_{S_B}\\M_{L_C},M_{S_C},m}}\langle L_AM_{L_A}S_AM_{S_A}|J_AM_{J_A}\rangle\langle L_BM_{L_B}S_BM_{S_B}|J_BM_{J_B}\rangle\langle L_CM_{L_C}S_CM_{S_C}|J_CM_{J_C}\rangle\\&\times\langle 1m1-m|00\rangle\langle\chi_{S_BM_{S_B}}^{14}\chi_{S_CM_{S_C}}^{32}|\chi_{S_AM_{S_A}}^{12}\chi_{1-m}^{34}\rangle[\langle\phi_B^{14}\phi_C^{32}|\phi_A^{12}\phi_0^{34}\rangle I(\vec{P},m_1,m_2,m_3)\\&+(-1)^{1+S_A+S_B+S_C}\langle\phi_B^{32}\phi_C^{14}|\phi_A^{12}\phi_0^{34}\rangle I(\vec{P},m_2,m_1,m_3)],\end{aligned} \tag{B4}$$

where M_{J_A}, M_{J_B}, and M_{J_C} denote the spin projections of each particles and the kinematic variables in the rest frame of the initial-state A are defined as

$$p_A=(m_V,0,0,0),\qquad p_B=(E_B,0,0,p_z),\qquad p_C=(E_C,0,0,-p_z). \tag{B5}$$

The overlap of the spin wave functions is

$$\langle \chi^{14}_{S_B M_{S_B}} \chi^{32}_{S_C M_{S_C}} | \chi^{12}_{S_A M_{S_A}} \chi^{34}_{1-m} \rangle = \sum_{S,M_S} \langle (j_1 j_4) S_B, (j_3 j_2) S_C; S M_S | (j_1 j_2) S_A, (j_3 j_4) 1; S M_S \rangle \times \langle S_B M_{S_B} S_C M_{S_C} | S M_S \rangle \langle S_A M_{S_A} 1 - m | S M_S \rangle. \quad \text{(B6)}$$

As we know, in the case of VVP, only the transversely polarized states of A will have nonvanishing contributions due to the antisymmetric tensor coupling. It is consistent with the fact that in the $^3P_0$ model the nonvanishing helicity amplitudes are just the $M_{J_A} M_{J_B} M_{J_C} = 110$ and $M_{J_A} M_{J_B} M_{J_C} = -1 - 10$. Similarly, we can analyze the VPP and VVV coupling in the quark model. The transition amplitudes calculated in the ELA and $^3P_0$ model, respectively, are listed in Table XIII. One can easily read the coupling relation:

$$g_{VPP} = \frac{m_V}{2} g_{VVP}, \quad \text{(B7)}$$

$$g_{VVV} = g_{VPP}. \quad \text{(B8)}$$

TABLE XIII. Relevant amplitudes in the $^3P_0$ model and ELA.

Amplitudes	$^3P_0$	ELA
$\phi \to K^+ K^-$		
$\mathcal{M}^{000}$	$\gamma \frac{1}{2\sqrt{3}} p_z$	$i g_{\phi K \bar{K}} 2 p_z$
$\phi \to K^{*+} K^-$		
$\mathcal{M}^{110}$	$\gamma \frac{-1}{2\sqrt{3}} p_z$	$-i g_{K^* \bar{K}} m_V p_z$
$\mathcal{M}^{-1-10}$	$\gamma \frac{1}{2\sqrt{3}} p_z$	$i g_{K^* \bar{K}} m_V p_z$
$\phi \to K^{*+} \bar{K}^{*-}$		
$\mathcal{M}^{110}$	$\gamma \frac{-1}{2\sqrt{3}} p_z$	$-i g_{\phi K^* \bar{K}^*} 2 p_z$
$\mathcal{M}^{-1-10}$	$\gamma \frac{-1}{2\sqrt{3}} p_z$	$-i g_{\phi K^* \bar{K}^*} 2 p_z$

Note that these two relations hold in the degenerate limit of V and P. In reality, they are broken by the mass differences between the V and P mesons. But for the purpose of constraining the number of free parameters, we can still adopt them in the analysis.

[1] P. A. Zyla *et al.* (Particle Data Group), Prog. Theor. Exp. Phys. **2020**, 083C01 (2020).
[2] P. H. Baillon *et al.*, Nuovo Cimento A **50**, 393 (1967).
[3] E. Klempt and A. Zaitsev, Phys. Rep. **454**, 1 (2007).
[4] Z. Bai *et al.* (MARK-III Collaboration), Phys. Rev. Lett. **65**, 2507 (1990).
[5] J. E. Augustin *et al.* (DM2 Collaboration), Phys. Rev. D **46**, 1951 (1992).
[6] F. Nichitiu *et al.* (OBELIX Collaboration), Phys. Lett. B **545**, 261 (2002).
[7] One notices that the masses and widths extracted from these three analyses [4–6] are very different.
[8] L. Faddeev, A. J. Niemi, and U. Wiedner, Phys. Rev. D **70**, 114033 (2004).
[9] J. F. Donoghue, K. Johnson, and B. A. Li, Phys. Lett. **99B**, 416 (1981).
[10] F. E. Close and S. Monaghan, Phys. Rev. D **23**, 2098 (1981).
[11] T. Barnes, F. E. Close, and S. Monaghan, Phys. Lett. **110B**, 159 (1982).
[12] F. E. Close, Rep. Prog. Phys. **51**, 833 (1988).
[13] C. Amsler and N. A. Tornqvist, Phys. Rep. **389**, 61 (2004).
[14] A. Masoni, C. Cicalo, and G. L. Usai, J. Phys. G **32**, R293 (2006).
[15] H. Y. Cheng, H. n. Li, and K. F. Liu, Phys. Rev. D **79**, 014024 (2009).
[16] Y. D. Tsai, H. n. Li, and Q. Zhao, Phys. Rev. D **85**, 034002 (2012).
[17] W. Qin, Q. Zhao, and X. H. Zhong, Phys. Rev. D **97**, 096002 (2018).
[18] Y. Chen *et al.*, Phys. Rev. D **73**, 014516 (2006).
[19] G. S. Bali, K. Schilling, A. Hulsebos, A. C. Irving, C. Michael, and P. W. Stephenson (UKQCD Collaboration), Phys. Lett. B **309**, 378 (1993).
[20] C. J. Morningstar and M. J. Peardon, Phys. Rev. D **60**, 034509 (1999).
[21] A. Chowdhury, A. Harindranath, and J. Maiti, Phys. Rev. D **91**, 074507 (2015).
[22] C. M. Richards, A. C. Irving, E. B. Gregory, and C. McNeile (UKQCD Collaboration), Phys. Rev. D **82**, 034501 (2010).
[23] W. Sun, L.-C. Gui, Y. Chen, M. Gong, C. Liu, Y.-B. Liu, Z. Liu, J.-P. Ma, and J.-B. Zhang, Chin. Phys. C **42**, 093103 (2018).
[24] M. Ablikim *et al.* (BESIII Collaboration), Phys. Rev. Lett. **107**, 182001 (2011).
[25] M. Ablikim *et al.* (BESIII Collaboration), Phys. Rev. Lett. **106**, 072002 (2011).
[26] M. Ablikim *et al.* (BESIII Collaboration), Phys. Rev. D **100**, 092003 (2019).
[27] M. Ablikim *et al.* (BESIII Collaboration), Phys. Rev. D **87**, 092006 (2013).
[28] M. Ablikim *et al.* (BESIII Collaboration), Phys. Rev. Lett. **108**, 182001 (2012).
[29] J. J. Wu, X. H. Liu, Q. Zhao, and B. S. Zou, Phys. Rev. Lett. **108**, 081803 (2012).
[30] L. D. Landau, Nucl. Phys. **13**, 181 (1959).
[31] R. E. Cutkosky, J. Math. Phys. (N.Y.) **1**, 429 (1960).
[32] G. Bonnevay, I. J. R. Aitchison, and J. S. Dowker, Nuovo Cimento **21**, 1001 (1961).

[33] R. F. Peierls, Phys. Rev. Lett. **6**, 641 (1961).
[34] X. G. Wu, J. J. Wu, Q. Zhao, and B. S. Zou, Phys. Rev. D **87**, 014023 (2013).
[35] F. Aceti, W. H. Liang, E. Oset, J. J. Wu, and B. S. Zou, Phys. Rev. D **86**, 114007 (2012).
[36] N. N. Achasov, A. A. Kozhevnikov, and G. N. Shestakov, Phys. Rev. D **92**, 036003 (2015).
[37] M. C. Du and Q. Zhao, Phys. Rev. D **100**, 036005 (2019).
[38] V. Mathieu and V. Vento, Phys. Rev. D **81**, 034004 (2010).
[39] G. Gabadadze, Phys. Rev. D **58**, 055003 (1998).
[40] J. Z. Bai *et al.* (BES Collaboration), Phys. Lett. B **594**, 47 (2004).
[41] M. Ablikim *et al.* (BESIII Collaboration), Phys. Rev. D **97**, 051101 (2018).
[42] N. Isgur, Phys. Rev. D **12**, 3770 (1975).
[43] Q. Zhao, G. Li, and C. H. Chang, Phys. Lett. B **645**, 173 (2007).
[44] G. Li, Q. Zhao, and C. H. Chang, J. Phys. G **35**, 055002 (2008).
[45] M. Tanabashi *et al.* (Particle Data Group), Phys. Rev. D **98**, 030001 (2018).
[46] T. H. Bauer, R. D. Spital, D. R. Yennie, and F. M. Pipkin, Rev. Mod. Phys. **50**, 261 (1978); **51**, 407(E) (1979).
[47] In principle, one can relate g_{XVP} to g_{XVV} in the $^3P_0$ model, which leads to $g_{XVV} \simeq 2g_{XVP}/m_X$. However, we find that this analytic relation is broken by about 30%. This is understandable since either K^* and $\bar{K}^*$ in the final state will be off shell and the form factor corrections would become significant.
[48] G. Li and Q. Zhao, Phys. Lett. B **670**, 55 (2008).
[49] A. Le Yaouanc, L. Oliver, O. Pene, and J. C. Raynal, Phys. Rev. D **8**, 2223 (1973).
[50] H. G. Blundell, arXiv:hep-ph/9608473.